Université du Québec
à Rimouski

EFFETS DU PROCESSUS DE FUSION DE POUDRE MÉTALLIQUE PAR LASER (L-PBF) SUR LES CARACTÉRISTIQUES DE LA POUDRE ET SUR LES PROPRIÉTÉS MÉCANIQUES DES PIÈCES IMPRIMÉES EN ACIER MARAGING

Mémoire présenté

dans le cadre du programme de maîtrise en ingénierie

en vue de l'obtention du grade de maître ès sciences appliquées

PAR
© RAYAN OTHMANE

Décembre 2022

Composition du jury :

Véronique Dassylva-Raymond, présidente du jury, Université de Québec à Rimouski

Jean Brousseau, directeur de recherche, Université de Québec à Rimouski

Abderrazak El Ouafi, codirecteur de recherche, Université de Québec à Rimouski

Vladimir Brailovski, examinateur externe, École de technologie supérieure

Dépôt initial le 27/10/2022 Dépôt final le 15/12/2022

DÉDICACE

A nos chers parents

A nos chers frères

A nos chères sœurs

A nos chers amis

A tous les enseignants et personnel de l'UQAR

A tous ceux qui ont participé à l'élaboration de ce travail

En témoignage de notre reconnaissance pour le soutien, la patience et les immenses sacrifices dont vous avez toujours fait preuve tout au long de nos études.

REMERCIEMENTS

Nous tenons à remercier dans un premier temps, toute l'équipe pédagogique de L'UQAR et les intervenants professionnels responsables de notre formation, particulièrement mon directeur de recherche M. Jean Brousseau pour son excellent encadrement.

Nous remercions également M. Abderrazak El Ouafi et M. Claude Belzile pour leurs orientations et leurs conseils pertinents. Nos sincères remerciements aux professionnels du département de mathématiques, d'informatique et de génie: M. Karel J. Uhlir, Mme Suzie Loubert, M. Charles-André Fraser, M. Dany Morin, M. Richard Lafrance et M. Jonathan Coudé.

Nous exprimons également nos remerciements au corps professionnel et administratif de l'UQAR pour leurs contributions à la réalisation de ce projet.

AVANT-PROPOS

La fabrication additive (impression 3D) est une nouvelle technologie de fabrication des pièces mécaniques par déposition de matière plastique ou métallique couche par couche sous contrôle par ordinateur. En dépit de tous les avantages offerts par cette technologie, en termes de complexité, d'intégralité des pièces et du rapport rigidité-légèreté, la validation des propriétés mécaniques des pièces imprimées constitue, jusqu'à présent, un véritable défi, surtout dans des secteurs industriels comme l'automobile et l'aérospatial. Parmi les technologies de la fabrication additive les plus reconnues, la technologie de fusion par laser (laser-powder bed fusion : L-PBF) est la plus utilisée. Elle consiste à étaler la poudre sur une plaque métallique pour être ensuite fusionnée couche par couche par laser jusqu'à la construction du modèle 3D de la pièce. La poudre non fusionnée est ensuite tamisée et recyclée pour lancer la prochaine impression. Toutefois, il est nécessaire de suivre l'évolution des caractéristiques de la poudre recyclée et d'étudier les facteurs qui influencent ses propriétés. Cette étude permet d'examiner les effets du processus de fusion sur les caractéristiques granulométriques et morphologiques de la poudre recyclée. Cela permet également de maîtriser et analyser l'évolution des propriétés de la poudre et leur impact sur les performances mécaniques des pièces imprimées en fonction du recyclage de la poudre.

RÉSUMÉ

Grâce à ses multiples avantages, l'impression 3D révolutionne les méthodes de fabrication traditionnelles. Elle permet la production des pièces mécaniques à géométrie très complexe, plus légères et très résistantes. Lors de l'impression d'une pièce, seule une partie de la poudre étalée est fusionnée. La poudre non fusionnée peut ensuite être tamisée et réutilisée. Cette étude porte sur les effets du procédé de fusion de la poudre (L-PBF) et du recyclage de la poudre sur les caractéristiques de la poudre d'acier maraging et sur les propriétés mécaniques des pièces. Ce mémoire est structuré autour des deux articles qui ont été rédigés dans le cadre du projet.

Le premier article présente les résultats de trois expériences relatives à l'analyse des effets du procédé de fusion sur les caractéristiques de la poudre. La première démontre que la taille des particules de poudre n'est pas uniforme dans le volume d'impression. Il est aussi démontré que la diminution de l'espacement entre les pièces imprimées change la distribution de la taille des particules (PSD) en augmentant la proportion de grosses particules. La dernière expérience montre que plus la structure des pièces en treillis est dense, plus le PSD et la morphologie du lit de poudre sont affectées. Ainsi, après douze cycles de recyclage, la taille des particules augmente et leur morphologie est dégradée.

Le deuxième article évalue les effets du recyclage de la poudre sur les propriétés mécaniques des pièces. Après 8 cycles d'impression, la taille des particules de poudre a augmenté, la morphologie des particules est changée et les propriétés en traction et en fatigue sont restées globalement constantes. Cependant, l'écart type de la limite d'endurance des éprouvettes fabriquées avec la poudre recyclée 8 fois est plus faible que celui obtenu avec les éprouvettes issues de la poudre neuve. Enfin, l'analyse fractographique montre que les pièces fabriquées à partir de la poudre recyclée présentent plus défauts d'impression que les pièces fabriquées avec de la poudre neuve.

.

Mots clés : Fabrication additive, procédé de fusion laser à lit de poudre (L-PBF), recyclage de la poudre, morphologie de la poudre, distribution de la taille des particules (PSD), pièces en treillis (lattices), éclaboussures.

ABSTRACT

Thanks to its multiple advantages, 3D printing is revolutionizing traditional manufacturing methods. It allows the production of light and strong mechanical parts with very complex geometry. During the printing process, only a portion of the spread powder is fused. The unfused powder can then be sieved and reused. This study focuses on the effects of the powder fusion (L-PBF) process on the characteristics of maraging steel powder and the effects of powder recycling on the mechanical properties of parts. This thesis is structured around the two papers that were written as part of the project.

The first paper presents the results of three experiments related to the analysis of the effects of the melting process on the characteristics of the powder. The first experiment shows that the particle size of the powder is not uniformly spread over the build plate. The second experiment shows among other things that decreasing the spacing between the printed parts changes the particle size distribution (PSD) and increases the proportion of large particles. The last experiment shows that the denser the structure of the lattice parts, the more the PSD and the morphology of the powder bed are affected. Moreover, after 12 reuse cycles, the particle size increased and the morphology of the powder degraded.

The second paper evaluates the effects of powder recycling on the mechanical properties of the parts. After eight printing cycles, the PSD of the powder has changed, the powder morphology is altered and the tensile and fatigue properties has remained globally constant. However, the standard deviation of the endurance limit of the specimens manufactured with powder recycled eight times is clearly lower than the one obtained with the specimens issued from the new powder. Finally, fractographic analysis shows that the parts made from the recycled powder have more printing defects than the parts made from virgin powder.

Keywords: Additive manufacturing, laser-powder-bed fusion (L-PBF) process, powder reuse, powder morphology, particles size distribution (PSD), lattice parts, spatters.

TABLE DES MATIÈRES

Dédicace vii

REMERCIEMENTS ix

AVANT-PROPOS xi

RÉSUMÉ xiii

ABSTRACT xv

TABLE DES MATIÈRES xvii

LISTE DES TABLEAUX xix

LISTE DES FIGURES xxi

LISTE DES ABRÉVIATIONS, DES SIGLES ET DES ACRONYMES xxv

LISTE DES SYMBOLES xxvii

INTRODUCTION GÉNÉRALE 1

CHAPITRE 1 L'ALTÉRATION DE LA POUDRE ACIER MARAGING CAUSÉE PAR LE PROCESSUS D'IMPRESSION 3D ET PAR LE RECYCLAGE DE LA POUDRE 13

1.1 RÉSUMÉ EN FRANÇAIS DU PREMIER ARTICLE 13

1.2 ALTÉRATION DE LA POUDRE EN ACIER MARAGING CAUSÉE PAR LE PROCESSUS D'IMPRESSION 3D ET PAR LE RECYCLAGE DE LA POUDRE 17

CHAPITRE 2 Effet du recyclage de la poudre d'acier maraging sur le comportement en traction et en fatigue des pièces fabriquées par le procédé de fusion de poudre par laser 48

2.1 RÉSUMÉ EN FRANÇAIS DU DEUXIÈME ARTICLE 48

2.2 EFFET DU RECYCLAGE DE LA POUDRE D'ACIER MARAGING SUR LES PROPRIÉTÉS EN TRACTION ET EN FATIGUE DES PIÈCES FABRIQUÉES PAR LE PROCÉDÉ DE FUSION DE POUDRE PAR LASER (L-PBF) 51

CONCLUSION GÉNÉRALE.....82
RÉFÉRENCES BIBLIOGRAPHIQUES.....86

LISTE DES TABLEAUX

Tableau 1: Composition chimique de l'acier maraging MS1 [4] 3

Tableau 2: Propriétés mécaniques des pièces en acier maraging MS1 [3, 4].....4

Tableau 3: Récaputilation des articles portant sur l'effet de recycle de la poudre 6

Table 1-1: Lattice dimension parameters.....26

Table 1-2: Diameter value variation along lines (toward right) and columns (toward bottom) 31

Table 2-1: The chemical composition MS1 virgin powder 59

Table 2-2: The tracking factors of 8 builds.....62

Table 2-3: Parameters of i and Mi using the Dixon and Mood method for cycle 1 71

Table 2-4: Parameters of i and Mi by Dixon and Mood method for cycle 8.....71

Table 2-5: Results of the staircase method 71

Table 2-6: Elemental composition of the inclusion presented in Fig.14 c) and surrounding metal (in mass percent).....74

Table 2-7: Elemental composition of the inclusion presented in Fig.14 (e, f) and surrounding metal (in mass percent) 74

LISTE DES FIGURES

Figure 1: Processus de fusion de poudre par laser (L-PBF) [1].....2

Figure 2: Machine EOS M290 (www.perfectionmachinery.com) 8

Figure 3: Méthode de recyclage de la poudre.....10

Figure 1-1. : PSD samples collected in different positions (matrix) over the build plate.. 24

Figure 1-2. : PSD samples relative to position of printed cylinder.....25

Figure 1-3. : Four concentric cylinders with increasing distance spacing.....25

Figure 1-4. : Lattices with different cell sizes 27

Figure 1-5. : PSD during printing cycle.....28

Figure 1-6. : D-values during a printing cycle.....29

Figure 1-7. : PSD samples collected in different positions (matrix) over the build plate. 30

Figure 1-8. : PSD measured in line i=1. 30

Figure 1-9. : D-value for line i=1.....31

Figure 1-10. : Location of powder samples collected along horizontal x-axis and vertical y-axis 33

Figure 1-11. : Cumulative PSD horizontal line. 34

Figure 1-12. : PSD horizontal line. 34

Figure 1-13. : D-value horizontal line (x-axis). 35

Figure 1-14. : PSD vertical line. 35

Figure 1-15. : Part with four concentric cylinders with increasing distance of spacing.....36

Figure 1-16. : Cumulative PSD measured for each zone.....37

Figure 1-17. : PSD measured for each zone 37

Figure 1-18. : D-value depending on distance spacing and zone 38

Figure 1-19. : PSD of lattices parts with different cell sizes. 40

Figure 1-20. : Percentage of larger particles (spatters) generated by lattices. 41

Figure 1-21. : D-value of lattices parts depending on area ratio.....41

Figure 1-22. : D-values of new powder versus powder reused 12 times. 42

Figure 1-23. : PSD of new powder versus powder reused 12 times. 42

Figure 1-24. : Morphologies of new powder. 44

Figure 1-25. : Morphologies of powder reused 12 times. 45

Figure 1-26. : Powder confined inside 3-mm-cell lattice. 45

Figure 1-27. : Heat-affected powder trapped in sieve device. 46

Figure 2-1. : Powder recycling method. 60

Figure 2-2. : Builds description 61

Figure 2-3. : Sector of powder consumption. 63

Figure 2-4. : Tensile specimen. Dimensions are in mm 63

Figure 2-5. : Fatigue specimen. Dimensions are in mm. 63

Figure 2-6. : The diameter values D-values over 8 printing cycles. 65

Figure 2-7. : Particle size distribution PSD over 8 reuse cycles.....66

Figure 2-8. : Morphologies of powder as observed using a scanning electron microscope. (A) virgin powder; (B) recycled 5 times; and (C) recycled 8 times. 67

Figure 2-9. : Surface roughness Ra of samples after 8 reuse cycles. 68

Figure 2-10. : Box plots of the average tensile properties versus reuse times: a) ultimate tensile strength, b) yield strength, c) Young module and d) elongation at break. 69

Figure 2-11. : Staircase test results of specimens printed in cycle 1 and cycle 8 70

Figure 2-12. : SEM images of the fracture surface of the first specimen printed in cycle 1 (S_a= 312 MPa , N= 415074); a) overview of the fracture surface at ×35, b) lack of fusion defect (LOF) at ×700. 72

Figure 2-13. : SEM images of the surface fracture of the 8th specimen printed in cycle 11 (S_a= 372 MPa , N= 297024); a) overview of the fracture surface at ×36, b) lack of fusion defect (LOF) at ×300. 72

Figure 2-14. : SEM images of the surface fracture of the first specimen printed in cycle 8 (S_a= 322 MPa , N= 63081) , a) overview of the fracture surface at ×36, b) LOF defect at ×300, c) LOF defect and inclusion at ×300, d) partially melted particles and LOF defect at ×200, e) inclusion defect (spatter) at ×1000, f) BSE mode of image e) at × 650. 73

Figure 2-15. : SEM images of the first surface fracture of the 10th specimen printed in cycle 8 (S_a=342 MPa , N= 152109), a) overview of the fracture surface at ×35, b) LOF defect at ×500, c) partially melted particle defect at ×650, d) LOF defect at ×400 , e) LOF defect, partially melted particles and gas pores at ×500, f) lack of fusion defects (crack origin) at ×300.....75

LISTE DES ABRÉVIATIONS, DES SIGLES ET DES ACRONYMES

AM	Additive Manufacturing (Fabrication additive)
L-PBF	Laser-Powder-Bed-Fusion (Fusion du lit de poudre par laser)
DED	Directed-Energy Deposition (Dépôt d'énergie dirigée)
EBM	Electron Beam Melting (Fusion par faisceau d'électrons)
PSD	Particle-size distribution (Distribution de taille des particules)
D-values	Diameter values (Valeurs de diamètre)
SEM	Scanning electron microscope (Microscope électronique)
CNC	Computer numerical control (Machine à commande numérique)
MS	Maraging steel (Acier Maraging)
UTS	Ultimate tensile strength (Limite de traction)
YS	Yield strength (Limite élastique)
LOF	Lack of fusion (Manque de fusion)
Fig	Figure (Figure)

LISTE DES SYMBOLES

Ø (mm)	Diameter (Diamètre)
d (mm)	Diameter (Diamètre)
Ra (µm)	Arithmetic mean surface roughness (Moyenne arithmétique des rugosités de surface)
Ɛ (%)	Strain at break (Déformation à la rupture)
ΔS (MPa)	Step size (Pas)
s (MPa)	Standard deviation (Écart type)
Sa (MPa)	Stress amplitude (Amplitude de la contrainte)
S_D **(MPa)**	Mean stress amplitude (Moyenne de l'amplitude de la contrainte)
F_{BA}	Standard deviation condition (Condition de l'écart type)
N	Number of cycles (Nombre de cycles)
K_t	Stress concentration factor (Coefficient concentration de la contrainte)
R	Fatigue stress ratio (Ratio des contraintes en fatigue)
C (mm)	Cell size (Taille de la cellule)
A $_{\text{filled}}$ (mm^2)	Total area of filled cylinders (Surface des cylindres pleins)
A $_{\text{lattice}}$ (mm^2)	Total area of lattice cylinders (Surface des cylindres en treillis)
V$_{\text{filled}}$ (mm^3)	Total volume of filled cylinders (Volume total des cylindres pleins)

$\mathbf{V}_{\text{lattice}}$ ($\boldsymbol{mm^3}$)	Total volume of lattice cylinders (Volume total des cylindres en treillis)
$\boldsymbol{R_A}$	Area ratio (Rapport de surface)
$\boldsymbol{R_V}$	Volume ratio (Rapport de volume)
$\boldsymbol{T_{las}}$ **(h)**	Laser operating time (Temps opérationnel du laser)
$\boldsymbol{T_{mach}}$ **(h)**	Machine operating time (Temps opérationnel de la machine)
$\boldsymbol{Q_{con}}$ **(kg)**	Powder melted and wasted after each cycle (Poudre fusionnée et perdue après chaque cycle)
$\mathbf{H_{max}}$ **(mm)**	Build's maximum height (Hauteur maximale de l'impression)
EDS	Dispersive X-ray spectrometer (Spectromètre dispersif à rayons X)

INTRODUCTION GÉNÉRALE

GÉNÉRALITÉ ET REVUE DE LITTÉRATURE

La fabrication additive (impression 3D) est une nouvelle technologie commandée par ordinateur qui consiste à fabriquer des pièces mécaniques par addition de matière (directed-energy deposition : DED) ou par fusion (laser-powder bed fusion : L-PBF) [1]. Elle a révolutionné les procédures traditionnelles de fabrication grâce à ses multiples avantages, en termes de performances mécaniques-légèretés, de complexité des géométries, de prototypage rapide et de rentabilité à long terme. L'un de ces avantages majeurs consiste à produire des pièces mécaniques de géométrie très complexe impossible à fabriquer avec les procédés traditionnels tout en garantissant un excellent rapport rigidité / légèreté. Grâce à cette technologie, il est possible d'intégrer plusieurs fonctions dans une même pièce plutôt que de fabriquer plusieurs pièces pour ensuite les assembler. Dans certaines conditions, cela permet de réduire le temps et le coût de fabrication et d'assemblage. De plus, les pertes de matière première sont normalement beaucoup plus petites que celles générées par les procédés d'usinage sous forme de copeaux [2]. Sans oublier que cette technologie permet de produire sur demande des pièces personnalisées, éliminant le coût de stockage et améliorant la chaîne d'approvisionnement [1]. Les technologies de la fabrication additive métallique sont de plus en plus déployées dans le domaine de l'automobile, l'aérospatial, l'aéronautique, le biomédical et les industries de fabrication d'outillage et de moulage [1]. Néanmoins, la fabrication additive fait face à certaines exigences, contraintes et limitations. Parmi ces contraintes, on peut parler de certaines opérations supplémentaires telles que le post-traitement qui introduit souvent des coûts additionnels à ceux de l'impression 3D. En effet, après l'impression, la poudre non fusionnée doit être tamisée, la pièce doit être retirée du plateau d'impression, subir des opérations de finition et traitée thermiquement pour réduire

les contraintes résiduelles, minimiser l'anisotropie et améliorer la tenue en service. Des opérations de finition par usinage sur la pièce sont très souvent nécessaires pour la rendre pièce complètement fonctionnelle, améliorer l'état de surface de certaines entités et lui donner l'apparence souhaitée [1].

Parmi les technologies de la fabrication additive, la technologie de fusion laser sur lit de poudre (laser-powder bed fusion) (L-PBF) occupe une place importante. Elle consiste à étaler la poudre sur un plateau de fabrication et de fusionner à l'aide d'un laser une couche à la fois jusqu'à la construction du modèle 3D. La figure 1 montre une représentation schématique illustrant les différentes composantes nécessaires au processus de fusion de poudre par laser [1].

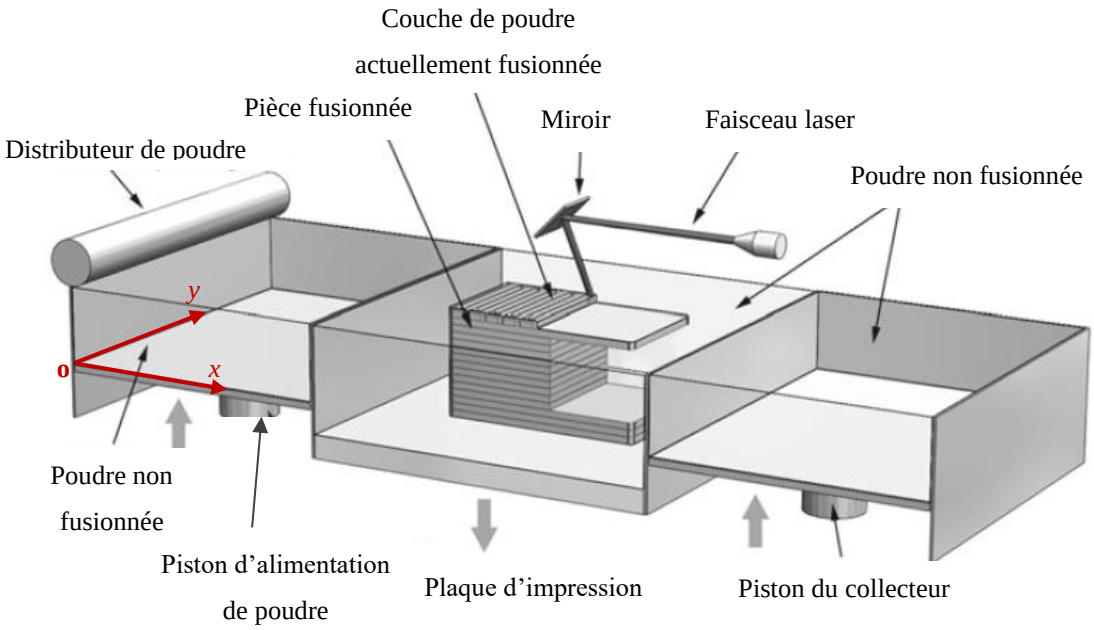

Figure 1: Processus de fusion de poudre par laser (L-PBF) [1]

Après l'impression, la poudre non fusionnée doit être recyclée en la passant à travers un tamiseur dans le but de filtrer les débris et les impuretés pour ensuite la recharger dans le compartiment de la poudre pour alimenter une nouvelle impression. Ce procédé de tamisage

est une option primordiale pour réduire le coût, souvent très élevé, de la poudre. Dans le cas où les pièces fabriquées ne sont pas destinées à des usages extrêmement sophistiqués, les fabricants peuvent choisir de réutiliser la poudre un certain nombre de cycles pour fabriquer des prototypes. Cependant dans le domaine de l'aérospatial, par exemple, il souvent exigé d'utiliser de la poudre neuve. La poudre doit posséder des caractéristiques optimales pour imprimer des pièces à fonctionnement critiques. Cela conduit à une augmentation significative du coût de fabrication. La poudre qui a déjà circulé dans la machine est alors utilisée pour des prototypes ou pour des composants non critiques.

Tel que présenté dans les tableaux 1 et 2, la poudre en acier maraging contient 0.03 % de carbone et possède une haute résistance à la traction et à la compression. La compagnie EOS recommande d'utiliser une homogénéisation à 940 ºC pendant 2 h suivie d'un refroidissement à l'air. EOS recommande aussi de faire subir aux pièces un vieillissement thermique à 490 ºC pendant 6 h puis un refroidissement à l'air. Après ce traitement, la dureté des pièces augmente de 30 HRC à 57 HRC [2, 3]. Différents composants aéronautique et aérospatial [4, 5], tels que les engrenages d'atterrissage, le crochet de l'arrêt de l'avion, les carcasses des turbomoteurs et les amortisseurs des robots lunaires sont fabriqués à partir de cet acier maraging. Dans le domaine de l'outillage, les fabricants commencent à imprimer des moules à injection et des noyaux intégrant des conduites de refroidissement à géométrie très complexe en acier maraging. Le coût de ce matériau est relativement élevé comparativement à d'autres aciers. Il coûte approximativement 140 US$ par kilogramme. Ce prix rend le recyclage de la poudre de l'acier maraging incontournable.

Tableau 1: Composition chimique de l'acier maraging MS1 [4]

Element	Fe	Ni	Co	Mo	Ti	Al.	Cr	Cu	C	Mn	Si	P	S
Max (%)	Balance	19	9.5	5.2	0.8	0.15	0.5	0.5	0.03	0.1	0.1	0.01	0.01
Min (%)		17	8.5	4.5	0.6	0.05	_	_	_	_	_	_	_

Tableau 2: Propriétés mécaniques des pièces en acier maraging MS1 [3, 4]

	Traitement thermique	
Direction d'impression	**Horizentale**	**Verticale**
Limite de résistance Rm (MPa)	2080	2080
Limite élastique 0.2% Re (MPa)	2010	2000
Déformation à la répture Ɛ (%)	4	4
La dureté (HRC)	50-57	

Les chercheurs s'intéressent de plus en plus à l'effet de recyclage sur les caractéristiques de la poudre et sur les propriétés mécaniques statiques et dynamiques des pièces imprimées. Ainsi, ils développent des nouvelles techniques pour contrôler l'évolution des propriétés de la poudre afin de répondre aux exigences des applications. Actuellement, les fournisseurs de la poudre ne donnent pas d'information relative sur l'effet du recyclage sur la poudre et sur les propriétés des pièces imprimées. La réponse à cette question n'est pas très simple. La qualité de la poudre recyclée dépend de plusieurs facteurs liés au procédé L-PBF. Les conditions environnementales extérieures telles que la température, l'humidité et le pourcentage d'oxygène influencent les caractéristiques de la poudre. D'autres facteurs tels que le nombre de cycles de recyclage, la géométrie de la pièce (géométrie simple ou structure en treillis), le volume des pièces imprimées par rapport au volume de poudre entendu et les paramètres du laser (puissance, vitesse, etc.) sont également à considérer [6-9]. Les différentes méthodes de tamisage et de mélange ont aussi un impact sur la poudre. On peut tamiser la poudre de façon manuelle ou automatisée sous gaz contrôlé. On peut aussi mélanger dans différentes proportions la poudre recyclée avec la poudre restante ou avec de la poudre neuve [10] . Tous ces facteurs influencent non seulement les caractéristiques physiques et chimiques de la poudre telles que la distribution de la taille des particules, la

morphologie des particules de poudre, la fluidité, la densité, la composition chimique, mais aussi la microstructure et les propriétés mécaniques des pièces imprimées (dureté, résistance mécanique, durée de vie en fatigue et état de surface) [11-15].

PROBLÉMATIQUE

Les caractéristiques de la poudre subissent des modifications à travers le processus d'impression. En conséquence, les propriétés mécaniques des pièces imprimées risquent de ne pas répondre aux exigences de fiabilité et de performance, notamment si la poudre est réutilisée à plusieurs reprises [6, 13, 16-23].

Jusqu'ici, peu d'études ont été menées sur le recyclage de la poudre. Les effets du recyclage de la poudre sur les propriétés mécaniques des pièces mécaniques ne sont pas définitivement établis. Comme le montre le tableau 3, il y a vraiment peu de recherches qui sont publiées sur le sujet du recyclage de la poudre d'acier maraging : Carrion [24] a conclu que le recyclage de la poudre en titane n'a pas d'effet sur les propriétés mécaniques. Cependant pour le comportement en fatigue, le recyclage améliore la durée de vie après l'usinage des pièces imprimées. Arash Soltani-Tehrani [25] affirme le même résultat pour la poudre en acier inoxydable 17-4 PH . Haokun Sun [14] a étudié l'effet du recyclage de la poudre d'acier maraging sur les propriétés mécaniques. Après avoir recyclé la poudre plus de cent fois, il constate que le recyclage n'influence pas les caractéristiques en traction des pièces imprimées. L'auteur n'a toutefois pas étudié l'effet de recyclage sur les propriétés en fatigue. Il est donc utile, justifiable et pertinent de s'intéresser à cette thématique afin d'apporter un éclairage sur quelques problèmes qui demeurent sans réponses malgré les études publiées en rapport avec ces questions.

Tableau 3: Récapitulation des articles portant sur l'effet de recyclage de la poudre

Matériau	Nombre d'articles qui ont étudié l'effet du recyclage de la poudre sur			Total des articles examinés dans cette étude
	Caractéristiques de poudre	Propriétés en statique	Propriétés en fatigue	
Titane Ti-6Al-4V	9	8	3	9
Acier inoxydable	5	5	2	5
Aluminium AlSi10Mg	2	2	1	2
Inconel 718	3	2	0	3
Maraging steel	1	1	0	1
Total	20	18	6	20

OBJECTIFS

L'objectif principal de cette étude consiste à investiguer les effets du processus de fusion de la poudre par laser (L-PBF) sur les caractéristiques de la poudre et sur les propriétés mécaniques des pièces imprimées à partir d'une poudre d'acier maraging recyclé. Plus spécifiquement :

1. Investiguer expérimentalement les facteurs et les conditions d'impression qui contribuent à la dégradation de la poudre en tenant compte de l'évolution de la taille et de la morphologie de la poudre lors du procédé d'impression L-PBF tout en considérant la proximité et les caractéristiques géométriques des pièces imprimées. Dans le cadre de cet objectif, nous imprimerons des pièces de géométrie simple et des structures de treillis et nous comparerons le niveau de dégradation de la poudre pour les différents types de pièces.

2. Analyser les effets du recyclage sur les caractéristiques granulométriques et morphologiques de la poudre et sur les propriétés mécaniques de traction et de fatigue des pièces imprimées en avec une poudre d'acier maraging.

MÉTHODOLOGIE

Ce projet vise à investiguer les effets du processus de fusion de la poudre par laser (L-PBF) sur les caractéristiques de la poudre et sur les propriétés mécaniques des pièces imprimées à partir de poudre métallique recyclée. Pour atteindre cet objectif, une méthodologie en deux phases expérimentales est adoptée. La première consiste à étudier les effets des facteurs et des conditions d'impression sur la dégradation de la qualité de la poudre. La seconde consiste à évaluer les effets de recyclage sur les propriétés mécaniques des pièces imprimées avec de la poudre recyclée. Les sections qui suivent décrivent les équipements, les matériaux, les conditions expérimentales considérés dans ce projet.

Machine de fabrication additive utilisée :

Les pièces ont été imprimées sur la machine EOS M290 400W dans une atmosphère d'azote avec une concentration d'oxygène inférieure à 1,3 % et une température de chambre de 40°C en utilisant le jeu de paramètres EOSPRINT MS1 040 performance M291 2.00. Dans ce jeu de paramètres, le diamètre du faisceau laser est 20 µm, la vitesse de construction est de 4,2 mm^3/s, l'épaisseur des couches est de 40 µm, l'espace de hachure (hatch offset) est égale à 6 µm et le motif laser est fixé à bandes tournées à 47º avec un angle de restriction de 30º après chaque couche.

Figure 2: Machine EOS M290 (www.perfectionmachinery.com)

Choix du matériau :

La poudre utilisée est l'acier maraging EOS MS1 (18% Ni maraging 300). Sa composition chimique est détaillée dans le tableau 1 selon la fiche technique du matériau (EOS art-no.9011-0016). La distribution de la taille des particules (PSD) a été mesurée par le granulomètre Malvern Panalytical Mastersizer 3000 équipé d'un module Hydro LV, selon la norme d'audit qualité QAS4002 de Malvern Panalytical et deux standards secondaires de poudre de silice avec un diamètre médian de 70 µm et 270 µm. De plus, la morphologie de la poudre a été analysée avec le microscope électronique à balayage (SEM) NanoImage SNE 4500M. La densité apparente de la poudre a été mesurée à l'aide d'une balance électronique et d'un bécher en plastique de 25 ml. La poudre est tamisée manuellement après chaque impression avec un tamis de 80 µm de taille.

Pré-traitement :

Pour améliorer leurs propriétés mécaniques, les éprouvettes imprimées ont été soumises à un vieillissement à 450°C pendant 6 heures, suivi d'un refroidissement à l'air ambiant. Ensuite, les éprouvettes de traction et de fatigue ont été usinées à l'aide de la machine CNC HAAS (VFO) - 3 axes.

Tests mécaniques :

Les essais de rugosité de surface ont été réalisés à l'aide d'un FORMATRACER SV-C3100/ 4100 de Mitutoyo. Les écarts moyens arithmétiques Ra de la rugosité du profil ont été mesurés sur trois éprouvettes de fatigue différentes pour chaque cycle d'impression. Cinq mesures linéaires de 2,5 mm de long ont été effectuées dans une direction parallèle à l'axe de l'échantillon, conformément à la norme OLDMIX. Les essais de traction ont été réalisés sur 3 éprouvettes pour chaque cycle, avec une vitesse d'allongement de 0,5 mm/min sur une machine servo-hydraulique MTS 810, à température ambiante, conformément à la norme ASTM E8. Lors des essais, un extensomètre MTS de modèle et de numéro de série 632.31F-24 et 315 a été utilisé. Les essais de fatigue sous contrôle de contrainte ont été réalisés à l'aide de la machine MTS 810 conformément à la norme ASTM E466-15, à température ambiante, en appliquant une charge sinusoïdale (Kt= 1 et R=0,1), en ajustant la fréquence à 25 Hz et en terminant les essais à 2×10^6 cycles s'il n'y avait pas de rupture. Finalement, l'analyse fractographique des surfaces de rupture est réalisée aussi avec le microscope NanoImage SNE 4500M. La composition chimique des éprouvettes a été déterminée à l'aide d'un spectromètre à rayons X à dispersion d'énergie (EDS) Bruker Esprit Compact couplé au microscope électronique à balayage NanoImage. Chaque spectre a été acquis pendant 120 secondes de temps réel à une tension d'accélération de 20 kV. Les éléments ont été automatiquement identifiés et quantifiés par le logiciel Esprit Compact et les résultats ont été normalisés à 100%.

Méthodologie expérimentale :

Pour étudier les effets du processus de fusion de la poudre L-PBF sur les caractéristiques granulométriques et morphologiques de la poudre, trois expériences ont été conduites : la première expérience vise à découvrir la taille de la poudre dans différentes positions sur le lit de poudre. La deuxième manipulation porte sur l'effet des éclaboussures générées par la fusion de la poudre sur la taille de la poudre et sur la variation de la distribution de la taille des particules de poudre selon la distance entre les pièces imprimées. La troisième expérience analyse l'altération de la poudre découlant de l'impression de formes

cylindriques constituées par des structures de treillis de différentes caractéristiques géométriques. Finalement, l'évolution des propriétés de la poudre après 12 cycles d'impression a été examinée.

Pour étudier l'effet du recyclage sur les propriétés mécaniques des pièces imprimées, huit impressions successives ont été effectuées, chacune contenant 4 éprouvettes pour les tests de traction, 17 éprouvettes pour le test de fatigue et 4 cylindres en treillis pour accélérer la contamination de la poudre. La hauteur des impressions diminuait à chaque cycle pour compenser la quantité de poudre consommée au cycle précédent et éviter d'ajouter la poudre neuve. Une fois l'impression terminée, la poudre était tamisée et on récoltait des échantillons de poudre pour analyser la distribution de la taille des particules (particule size distribution, PSD), la morphologie de la poudre et la densité apparente. Après on rechargeait la poudre dans le distributeur de poudre et l'impression suivante était lancée. Une fois les huit impressions complétées, les tests de traction et de fatigue ont été appliqués sur les éprouvettes imprimées. Finalement, une analyse fractographique a été conduite sur les éprouvettes cassées durant les tests de fatigue. Cela a permis d'investiguer les causes possibles de fracture. La figure 3 résume la méthode de recyclage de la poudre déployée.

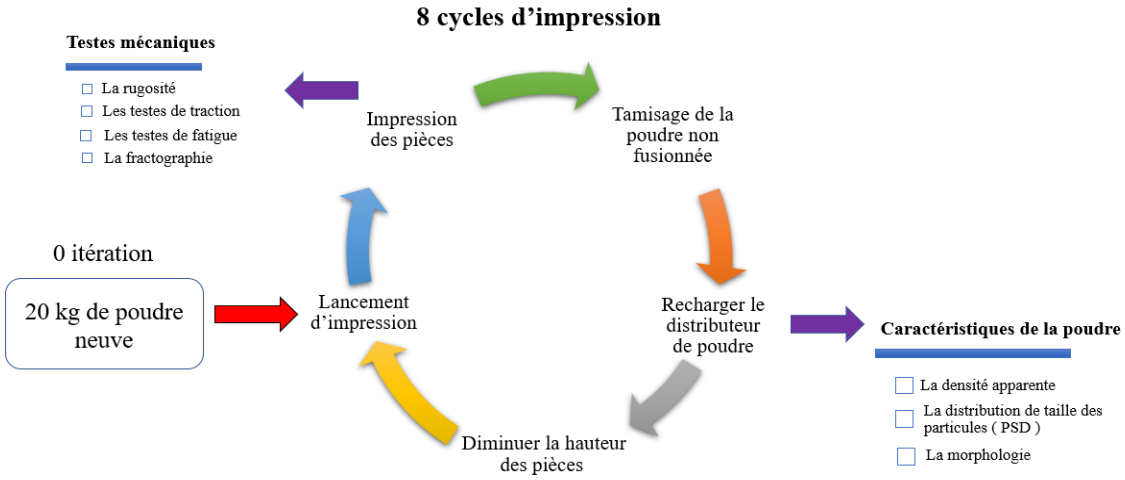

Figure 3 : Méthode de recyclage de la poudre

ORGANISATION DU MÉMOIRE

Le mémoire est composé d'une introduction générale, de deux chapitres sous forme d'articles et d'une conclusion générale. Le chapitre 1 définit le contexte, présente les principaux éléments et concepts ayant un rapport direct avec le sujet de recherche. Il présente également une brève revue de littérature, pose la problématique à traiter, identifie les objectifs à atteindre et décrit l'approche méthodologique proposée. Le premier article traite les effets du procédé de fusion de poudre L-PBF sur les caractéristiques granulométriques et morphologiques de la poudre. Le deuxième article aborde l'effet de recyclage sur les propriétés de la poudre et sur les performances mécaniques des pièces imprimées en acier maraging. Finalement, la conclusion générale revient sur la problématique et sur les objectifs en faisant le lien avec les résultats obtenus et les observations constatées tout en proposant des pistes à considérer pour une poursuite éventuelle de ce projet de recherche.

CHAPITRE 1
L'ALTÉRATION DE LA POUDRE ACIER MARAGING CAUSÉE PAR LE PROCESSUS D'IMPRESSION 3D ET PAR LE RECYCLAGE DE LA POUDRE

1.1 RÉSUMÉ EN FRANÇAIS DU PREMIER ARTICLE

La fabrication additive métallique (FAM) est une nouvelle technologie de fabrication des pièces mécaniques. Elle permet de produire des pièces géométriquement très complexes impossibles à produire avec les méthodes traditionnelles de fabrication. De nos jours, plusieurs secteurs comptent sur cette technologie pour développer leurs produits, notamment les secteurs de l'aérospatiale, de l'automobile et du biomédical. La technologie de fusion de la poudre métallique par le laser (laser powder bed fusion : L-PBF) est la plus utilisée. Cependant, la poudre est susceptible de subir des modifications suite au processus d'impression, de stockage et de tamisage qui peuvent conduire à la dégradation de ses caractéristiques intrinsèques. L'objectif de cet article est d'examiner l'impact du processus d'impression sur la dégradation de la poudre.

L'article expose les résultats issus de trois expériences. La première vise à évaluer la taille de la poudre selon la position sur la plaque d'impression. Les résultats ont montré que la taille des particules du lit de poudre n'est pas uniformément distribuée. L'analyse des échantillons de poudre montre que la taille des particules diminue légèrement après le tamisage.

La deuxième expérimentation avait comme objectif d'examiner l'effet d'une pièce imprimée sur la distribution de la taille de la poudre (contamination simple). Cette expérience montre la présence d'éclaboussures suivant la ligne verticale Oy (voir figure 1) et de particules noires qui sont localisés en dessous de la pièce imprimée. Cependant leur présence n'a pas introduit de changement dans la distribution de la taille des particules (PSD).

Toutefois, le long de la ligne horizontale Ox (voir figure 1), les particules proches du collecteur sont en moyenne plus grosses que les particules positionnées proche du distributeur. Ensuite, on a investigué la variation de la taille des particules de poudre en fonction de la distance entre les pièces (contamination croisée). On a constaté qu'au fur et à mesure que cette distance diminue, la proportion des fines particules baisse et celle des grosses particules augmente. Cela indique que plus l'échantillon de poudre est récolté proche du bain de fusion, plus les grosses particules sont prédominantes. Cette augmentation de la taille des particules peut être justifiée par les agglomérations causées par les éclaboussures.

La troisième expérience a pour objectif d'analyser l'altération et la dégradation de la poudre lorsqu'on imprime des cylindres en treillis (lattices) de différentes tailles de la maille. Les observations montrent que lorsque la taille de la maille augmente de 2 mm à 5 mm, le PSD est déplacée à gauche, indiquant une augmentation de la proportion des fines particules et une légère diminution des grosses particules. Il est également à noter que lorsque la taille de maille des treillis augmente de 2 mm à 5 mm, le pourcentage des grosses particules dont le diamètre est supérieur à 1 mm augmente de 1.4 % à 6.5 % respectivement. Cependant, ces grosses particules ne sont détectées ni dans la nouvelle poudre ni dans la poudre tamisée. On peut supposer que les agglomérations causées par les éclaboussures expliquent ce changement. Les images microscopiques ont confirmé ces résultats.

Grâce à ces trois expériences, on peut confirmer que la poudre n'est pas uniformément étalée sur le plateau d'impression et que le processus du tamisage a un effet négligeable sur la distribution de la taille de la poudre durant un seul cycle d'impression. Il est également démontré que l'impression d'une pièce génère des fumées et des résidus qui sont transportées par le flux de gaz du haut vers le bas suivant la direction inverse de Oy (voir figure 1) du lit de poudre. Cependant, leurs effets sur la taille du lit de poudre sont négligeables. De plus, la distance entre les pièces imprimées altère la taille du lit de poudre. En effet, plus les pièces imprimées sont proches les unes des autres et plus la présence des grosses particules dans la poudre est prédominante. En outre, il est confirmé que les caractéristiques géométriques des pièces imprimées en treillis altèrent les propriétés de la poudre figée à l'intérieure des treillis,

particulièrement la taille et la morphologie. Finalement, la taille de poudre tamisée augmente après 12 cycles d'impression, et la morphologie des particules a été affectées par la présence des agrégats et des particules partiellement fusionnées ou déformées.

Cet article, intitulé « Maraging Steel Powder Alteration Caused by 3D Printing Process and Powder Recycling », a été soumis le 07/10/2022 au journal *Heliyon*. En tant que premier auteur, j'ai contribué à l'essentiel de la recherche sur l'état de la question, au développement de la méthode et à l'exécution des travaux expérimentaux. Le professeur Jean Brousseau, second auteur, a fourni l'idée originale, a aidé à la recherche sur l'état de la question, a contribué au développement de la méthode ainsi qu'à la révision de l'article. M. Claude Belzile a participé à l'exécution des tests d'analyse des propriétés de la poudre et M. Abderrazak El Ouafi a contribué à la planification des expériences et à la révision de l'article.

1.2 ALTÉRATION DE LA POUDRE EN ACIER MARAGING CAUSÉE PAR LE PROCESSUS D'IMPRESSION 3D ET PAR LE RECYCLAGE DE LA POUDRE

Maraging Steel Powder Alteration Caused by 3D Printing Process and Powder Recycling

Othmane Rayan[a], Jean Brousseau[a], Claude Belzile[b], Abderrazak El Ouafi[a]

[a] Department of Mathematics, Computer Science and Engineering, Université du Québec à Rimouski (UQAR), 300, allée des Ursulines, C.P. 3300, Rimouski, QC G5L 3A1, Canada.
[b] Institut des sciences de la mer de Rimouski (ISMER), Université du Québec à Rimouski, 310 allée des Ursulines, Rimouski, QC, G5L 3A1, Canada.

ABSTRACT:

Metallic additive manufacturing (AM) technologies have recently drawn a lot of interest, notably in the aerospace, automotive, and biomedical fields, as they allow a great degree of design flexibility, perform well mechanically, and reduce material waste. As long as the unfused powder is sieved and recycled for the next print, AM is a green and clean process. However, the recycled powder is prone to several modifications during the course of printing that may affect the mechanical properties of finished components. The study examines the phenomenon of powder degradation caused by laser powder bed fusion (L-PBF) printing process and the reuse of the powder. The experiments were conducted on a laser powder bed fusion printer. Maraging steel was chosen because there are very few studies on the alteration of this type of powder. The effects of part location, distance between parts, lattice structure on powder characteristics are investigated. Results show that powder particles are not uniformly distributed over the powder bed, coarsening toward the collecting bin. Nevertheless, the gas filtration system that transports spatters and fumes has no

noticeable effect on the powder bed particle-size distribution (PSD). Analyses of the powder spread over the build plate reveal that the PSD shifts toward larger particles with a considerable drop in the percentage of fine particles as the spacing between printed parts is decreased. Printing lattice structures have a substantial impact on the PSD of the powder bed and produced a huge number of spatters, aggregates, ‘‘Clip-Clap”, elongated particles, broken particles, shattered and deformed particles. As the study shows, the PSD of the powder became coarser and their particles morphology was altered after 12 reuses.

1. Introduction:

Additive manufacturing (AM) is a novel technique used to create 3D products from virtual 3D models by layering the component until the part is complete. The earliest AM concept was a topographical map produced at the end of the nineteenth century [1]. Now, additive manufacturing knowledge and technologies are widely developed and advanced. They allow us to produce innovative components that were previously impossible to make. In the biomedical sector, surgeons currently replace various human body components with 3D parts [1, 26].

Laser powder bed fusion (L-PBF) and electron beam melting (EBM) are the most commonly used metallic additive manufacturing technologies. Both use the same printing process[1]. It begins by spreading a fine layer of powder across the build plate. Then, either a laser or an electron beam melts the powder. Next, the build platform descends to allow the next layer of powder to be spread and melted, and this cycle repeats until the 3D part is complete. The difference between these two technologies is the energy source: L-PBF uses a laser to melt the powder, whereas EBM requires an electron beam [1]. The main methods used to produce AM powders are gas atomization, induction melted bar atomization, plasma atomized wire, plasma rotating electrode atomization and water atomization, among others. Each process has advantages and disadvantages in terms of powder properties. For example, water atomization produces particles with irregular shapes and wetness [6, 27, 28]. Herzog *et al*. [29] also reported an increase in oxygen content associated with powder produced by water atomization, whereas the gas atomization process reduces the risk of oxidation and

contamination [29-31]. Plasma atomized wire produces a high quality powder with a high ratio of spherical particles, high powder density and low porosity [23, 27].

The printing process itself has a significant impact on powder features, particularly the particle size distribution (PSD), chemical composition and morphology. When a laser melts the powder, it produces spatters and heat-affected particles, which deposit on the powder bed, affecting the nearby portion of the powder bed [15, 22]. This is especially the case when printing lattice parts, which offer the multiple advantages of energy absorption, lightweight construction, excellent mechanical and thermal properties, and reduction of material consumption [32]. However, it has been argued that printing this type of structure accelerates powder bed contamination and degradation by producing a considerable number of spatters [16] .

Anwar and Pham [12] studied the effects of inert gas flow velocity and scanning direction on the formation and accumulation of spattered powder. Their research shows that flow velocity affects the accumulation of spatters on the build plate. They also underline that scanning in the direction of the gas flow significantly decreases the accumulation of spatters over the powder bed. The presence of spatters on the powder bed must be minimized as much as possible since it not only increases the percentage of porosity within the printed component, but is also responsible for modifying the morphology of recycled powder [19]. According to Popov *et al*. [33], the mechanical deformation of particle shape is largely caused by laser heat exposure which welds satellites to particles. Renishaw [34] also confirmed this result. Furthermore, Popov *et al*. [33] claimed that satellites exist in virgin powder, but that the bonding of satellites with particles, which produces agglomerations, is induced by the sieving process. Rock *et al*. [35] also investigated the impact of spatters on PSD and particle morphology. They concluded that the particle morphology of virgin powder differs significantly from that of powder recycled 10 times. They also discovered that, despite the fact that the sieving process removes the majority of spatters, some do infiltrate the feedstock powder. Consequently, the spatters are extremely likely to affect the powder and the mechanical properties of the manufactured part. Rock *et al*. [35] and Anwar and Pham [12] both claimed that despite the gas flow effect, spatters can

become candidates for melting and incorporation into a component if ejected into a laser pattern.

Moreover, according to Sutton *et al*. [15], laser spatters and solidified particles, also known as ejecta or heat-affected powder, are responsible for compromising the morphological and chemical properties of reused powder. Spatters not only contaminate the powder bed when they are ejected, but also affect the mechanical properties of the next part printed when they are deposited over its laser pattern. Furthermore, the very small spatters traveling through the sieve device can influence the morphology of recycled powder and increase its oxygen concentration. In addition, Tan *et al*. [6] explained a defect called the balling effect that occurs in the L-PBF printing process when laser power is not properly adjusted. Balling affects melt pool formation and produces partially melted powder. Consequently, it enhances porosity inside parts and affects their surface roughness. Furthermore, Powell *et al*. [8] showed that the handling and removal procedure can impact powder properties. The unfused powder can be easily polluted by impurities like fibers, dust and other pollutants transported by ambient air during the handling, cleaning, and sieving processes. Thus, when sieve devices and procedures are not effective, the sieved powder can be polluted. Contamination can also be caused by the presence of foreign material in the dispenser. For example, after a material change, some particles of the previous material can be mixed with the newly loaded material. Soundarapandiyan [7] reported a severe contamination scenario caused by the presence of Inconnel 625 particles in the aluminum powder sample, which resulted in mechanical component failure. Storage techniques are also critical for preserving powder quality. When a reactive powder is not stored in an inert atmosphere, particles are more likely to come into contact with the ambient air. As a result, the powder is exposed to corrosion, oxidation, and contamination [8]. Aside from these factors, the chemical properties of the powder change significantly after multiple reuse cycles. Tang *et al*. [36] observed an increase in oxygen content while aluminum and vanadium percentages remained stable in Ti-6Al-4V powder after 21 printing cycles on an EBM machine. Popov *et al*. [33] also observed oxygen pickup in titanium powder exceeding the maximum ASTM F2924-14 (2014a) standard after 69 prints in an EBM process.

Renishaw [34] validated prior findings for the same material in a selective laser melting (SLM) process across 38 cycles, with an increase in oxygen and nitrogen content exceeding titanium Grade 23 standards. It is also worth noting the change in powder particle size that occurs due to reusing powder. O'Leary *et al*. [37] noticed a significant drop in the proportion of fine particles less than 15 µm in diameter and an increase in the number of larger particles over 45 µm in diameter after recycling Ti-6Al-4V powder 5 times in an L-PBF process. They also observed that powder surfaces became rougher and less spherical. Similar results were achieved with AISI 304L stainless steel powder by Sutton *et al*. [38] who revealed an increase in particle diameters after 5 reuse cycles. Continuous refreshing or collective aging are two recycling techniques used in AM. In powder refreshing, the quality of recycled powder is determined by the percentages of virgin and reused powder utilized in the mix. Tan *et al*. [22] showed that combining 75% virgin powder with 25% reused powder results in an excellent flowability that is comparable to 100% virgin powder. In the collective aging technique, the depositing and mixing methodologies for combining dispenser powder with reused powder have a substantial impact on the quality of printed components [10].

It is crucial to emphasize that changes in physical powder characteristics, specifically particle size distribution (PSD) and morphology, have an impact on both the rheological powder characteristics and the mechanical performances of completed parts [17, 24, 36]. Brika *et al*. [39] investigated the impact of geometrical particle characteristics on both the rheological properties and mechanical performances of printed parts. Their research showed that using extremely spherical powders substantially improved powder flowability, powder density, and part density. It also increased mechanical properties, namely ultimate tensile strength, and yield strength, as well as surface roughness and dimension accuracy. Furthermore, Liu *et al*. [40] reported that variation in powder particle size distribution was responsible for differences in powder quality and mechanical properties. Powder with a wide PSD provides better powder bed density, higher density parts under low laser energy intensity, and smoother surface finishing on components, while a powder with a narrower PSD has better flowability and produces components with optimal tensile properties and hardness. Moreover, it has been demonstrated that powder properties are not uniform

throughout all regions of the powder bed. Pal *et al*. [11] investigated the evolution of L-PBF Ti–6Al–4V and Co–Cr–W–Mo powder characteristics and mechanical properties of specimens printed in two different locations over the build plate. For both materials, powder near the dispenser (position 1) had more fine particles and a better spherical shape than powder near the collecting bin (position 2). Parts printed in position 1 showed greater density and smaller pores, resulting in higher tensile properties than specimens printed in position 2.

The aforementioned studies revealed changes in powder characteristics and mechanical qualities of manufactured components caused by the additive manufacturing process itself, particularly powder degradation induced by laser heat exposure and powder reuse cycles. However, in the literature published to date, the influence of the geometry of printed parts as well as their positions over the build plate on the evolution of powder characteristics remains unclear and less discussed. Therefore, the present research investigates the influence of part geometry, part location and proximity of the printed parts on the contamination of the powder bed and on the recycled powder. The study also examines the extent to which lattice structures speed up powder degradation. In the experiments, maraging steel powder was used mainly because there are very few studies on the contamination and recycling of this material. It was relevant to examine how maraging steel powder behaves under the effect of the printing process.

2. Materials and experimental program:

2.1. Materials:

All components are printed with maraging steel MS1 on an EOS M290 400W machine, in an azote environment with less than 1.3 percent oxygen concentration and a chamber temperature of 40°C. The EOSPRINT template used was MS1 040 performance M291 2.00. After each print, the powder was sieved manually through an 80 µm mesh sieve and fed into the dispenser.

The powder samples were analyzed with a Malvern Panalytical Mastersizer 3000 particle-size analyzer equipped with a Hydro LV module. The stirrer speed was set to 3000

rpm, a speed sufficient to keep the particles in suspension. Prior to the measurements, the sample was submitted for 60 s to Hydro LV ultrasounds at 25% power to help disintegrate aggregates. Three consecutive measurements of 30 s each (20 s with the red laser plus 10 s with the blue LED) were collected for each sample. The average statistics of the three measurements were computed (the coefficient of variation in Dv10, Dv50 and Dv90 of the three measurements was always <1%, indicating a good sample dispersion). The Mastersizer general purpose optical model for non-spherical particles was employed with a refractive index of 2.757 and absorption 1.0 for stainless steel (values taken from the Malvern Panalytical database included with Mastersizer 3000 software). Instrument performance was confirmed using Malvern Panalytical's QAS4002 Quality Audit Standard and two silica powder secondary standards with median diameters of 70 µm and 270 µm. In addition, the powder morphology was analyzed with a NanoImage SNE 4500M scanning electron microscope. Three experiments were conducted to investigate alterations in powder PSD throughout the L-PBF printing process, studying the effects on PSD of gas flow transporting spatters, powder distance from the printed part, and geometrical properties of lattice cylinders.

2.2. Experimental program:

2.2.1. Experiment 1: PSD variation caused by the powder spread process

The first experiment examines the particle size distribution (PSD) of the powder spread over the build plate during a printing cycle at different locations. The PSD of powder loaded in the dispenser (before printing) was compared with, powder at 16 different sites (matrix) over the powder bed, powder accumulated in the collector bin, and powder after sieving. To do so, we printed at x=125 mm and y=10 mm a small vertical cylinder of Ø=10 mm and h=20 mm. The cylinder was located outside the sample matrix and close to the gas outlet, as shown in Figure 1-1.

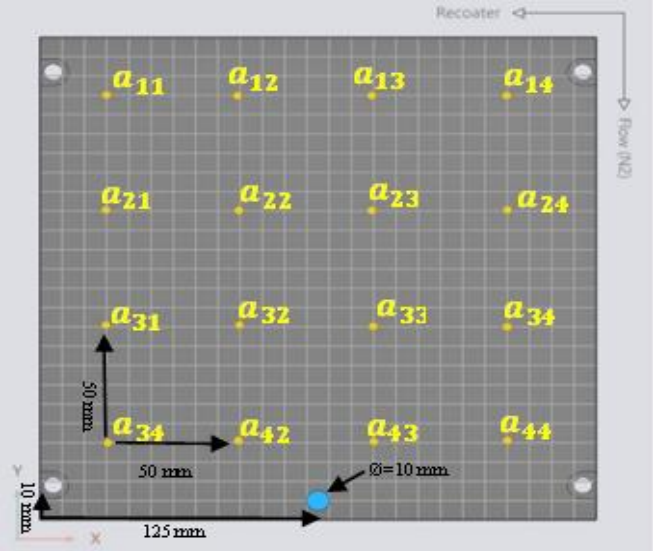

Figure 1-1: PSD samples collected in different positions (matrix) over the build plate

2.2.2. Experiment 2: PSD variation depending on the position of printed part

Experiment 2A: Single contamination

Experiment 2A evaluates the particle size distribution (PSD) based on horizontal and vertical distances from a centrally located printed cylinder of 50 mm in diameter and 20 mm in height. The printing process generates spatters and smoke that contaminate the power bed. As shown in Figure 1-2, the 12 samples collected are 40 mm apart.

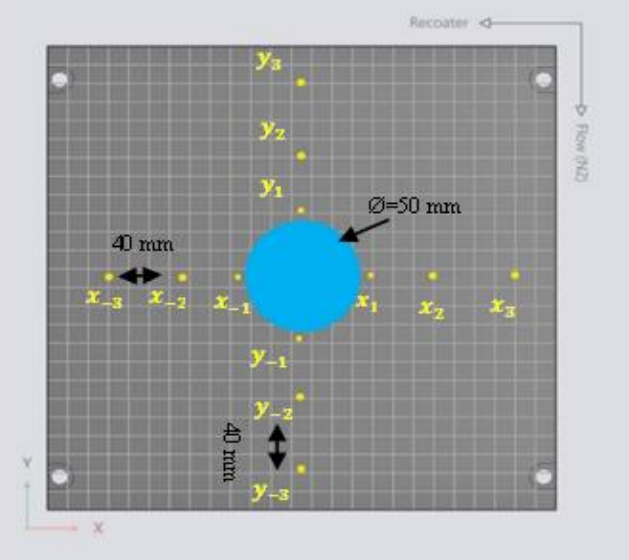

Figure 1-2: PSD samples relative to position of printed cylinder

Experience 2B: Double contamination

To study double contamination, four concentric cylinders were printed, then the PSD of the powder collected in four different zones as shown in Figure 1-3 was analyzed.

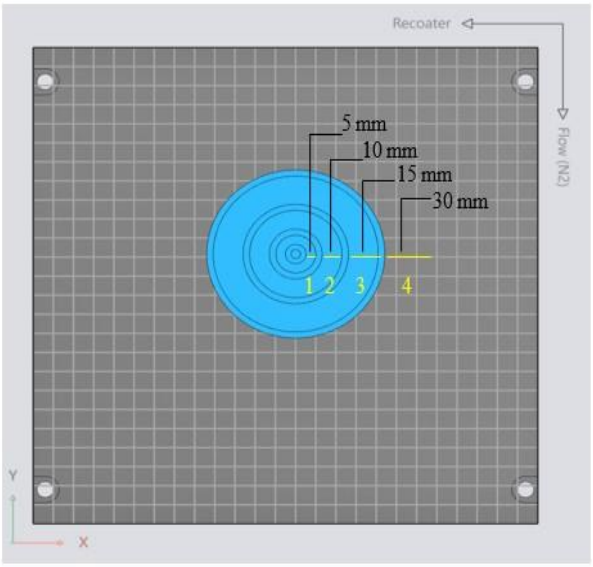

Figure 1-3: Four concentric cylinders with increasing distance spacing

2.2.3. Experiment 3: PSD changes when printing lattice structures of different cell sizes

The third experiment highlights the evolution of particle size distribution (PSD) and morphology of powder depending on the area and volume ratios of printed parts. For this experiment, lattice cylinders were designed using nTopology software. The area and volume ratios of a lattice cylinder were defined as follows:

Area ratio: $R_A = A_{lattice} / A_{filled}$ (1), Volume ratio: $R_V = V_{lattice} / V_{filled}$ (2).

Where A_{filled}, $A_{lattice}$, V_{filled} and $V_{lattice}$ are respectively the total area or volume of filled or lattice cylinders of equal diameter and height.

In this final experiment, we investigated the PSD of powder contained inside 4 lattice cylinders with the same diameter of Ø = 50 mm but four different cell sizes: 2 mm, 3 mm, 4 mm, and 5 mm for cylinders 1, 2, 3, and 4, respectively (see Figure 1-4). The lattice cylinders were created with nTopology software using a cube edge structure with fillet radius of 2.1 mm and thickness of 0.5 mm. It is important to note that when the cell size was increased from 2 mm to 5 mm, the area and volume ratios dropped. Table 1-1 presents the characteristics of the four lattice cylinders.

Table 1-1 : Lattice dimension parameters

Lattice cylinder	Cell size C (mm)	Area ratio Ra	Volume ratio Rv
1	2	8.4	0.49
2	3	5.7	0.42
3	4	3.6	0.26
4	5	2.4	0.18

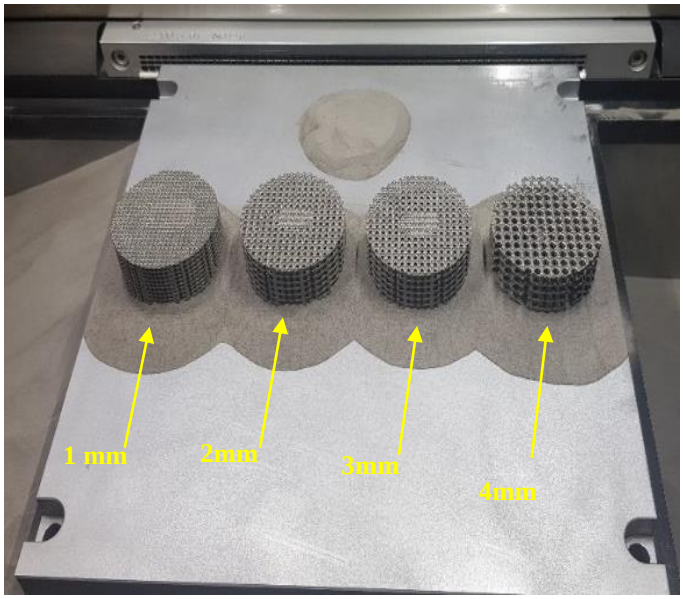

Figure 1-4: Lattices with different cell sizes

3. Results and discussion:

3.1. Results of Experiment 1: PSD analyzed during printing cycle

Two samples of powder were collected from the dispenser before printing, two after printing and sieving, and two more from the collector bin, which contains the excess powder displaced by the recoater. The powder in the collector and the unfused powder on the build plate were sieved and placed in the dispenser. As shown in Figure 1-5, the PSD of the three samples is very similar, but it can be observed that the dispenser powder moves slightly to the left in the direction of smaller particles after printing and sieving, while the PSD measured in the collector is located between the other two PSD arcs. Figure 1-6 shows that after the sieving process, the diameter D-values of the dispenser powder D90, D50, and D10 decrease by 3.7%, 4%, and 6.8%, respectively, while the D-values of the collector powder appear to

be quite similar to the D-value of the dispenser powder before printing. Consequently, the powder size in the dispenser during a printing cycle remains approximately constant when printing a small part. This change can be partly attributed to the fact that the powder is poured through a sieve with an 80 µm mesh, so that coarse particles (> 80 µm) are retained in the sieve and eliminated from the process [24]. It should also be noted that during the printing process, splashes can weld particles together. Some particle agglomerations do not pass through the sieve mesh, which changes the PSD of the powder.

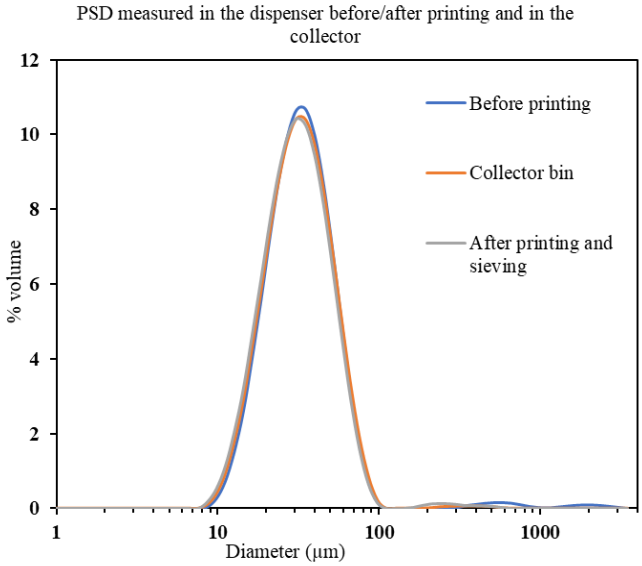

Figure 1-5: PSD during printing cycle

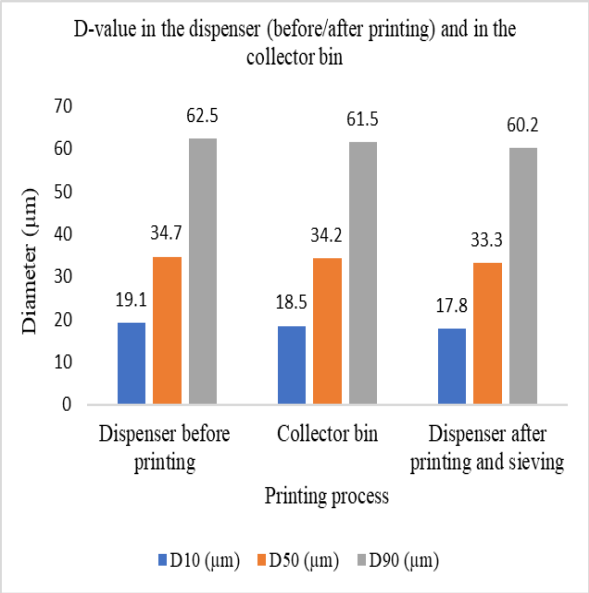

Figure 1-6: D-values during a printing cycle

The powder samples from 16 locations (matrix) were collected over the powder bed (Figure 1-7). Figures 1-8 and 1-9 present the PSD and D-values, respectively, along the horizontal line i=1. As can be observed, along the horizontal line, the PSD slightly displaces left toward the fine particles as we move from the collector to the dispenser. These results become more apparent in the D-value graphs, which show that the D90, D50, and D10 values gradually decline as they move horizontally rightward toward the dispenser. The results are similar for the other three lines. The D50 value, for example, varies for each horizontal line (i = 1, 2, 3, 4) by -9.8%, -10.8%, -9.6% and -14.6%, respectively. However, from the top to the bottom of the powder bed, the vertical columns show a mild reduction in D-values with the exception of column j = 4 (see Table 1-2). For example, the variation in D50 for vertical columns j = 1, 2, 3, 4 is -4.5%, +1.6%, -4.8%, and -9.5%, respectively.

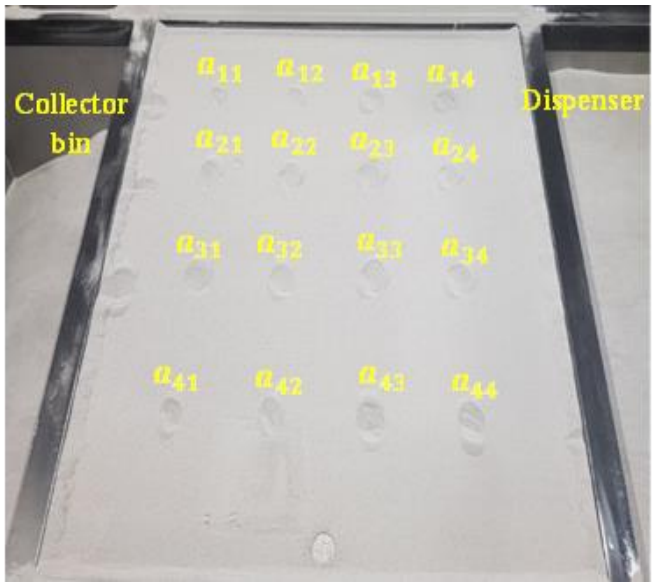

Figure 1-7: PSD samples collected in different positions (matrix) over the build plate

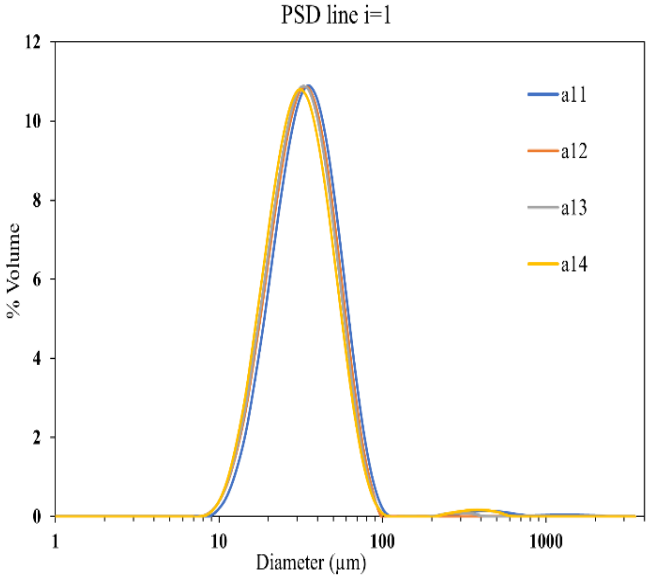

Figure 1-8: PSD measured in line i=1

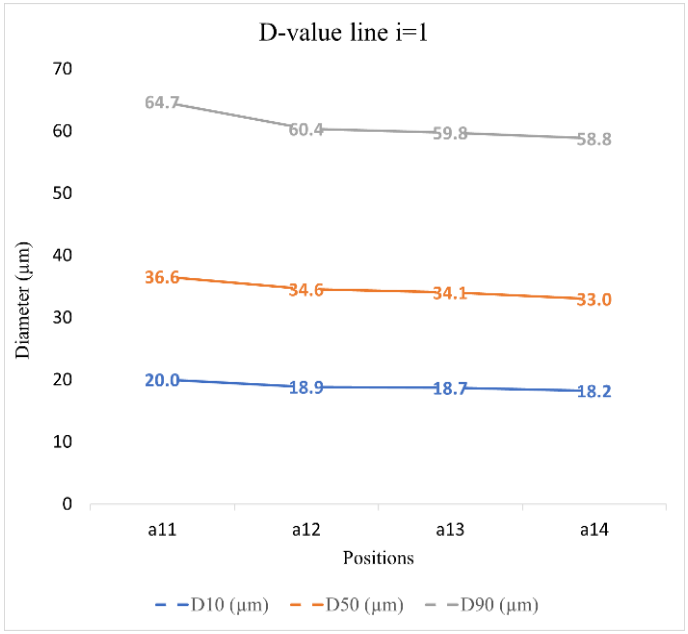

Figure 1-9: D-value for line i=1

Table 1-2: Diameter value variation along lines (toward right) and columns (toward bottom)

	Position	Δ D10(µm)	Δ D50(µm)	Δ D90(µm)
Line	i=1	-9.0%	-9.8%	-9.1%
	i=2	-12.1%	-10.8%	-8.0%
	i=3	-6.3%	-9.6%	-10.9%
	i=4	-14.1%	-14.6%	-12.2%
Column	j=1	-4.9%	-4.5%	-3.5%
	j=2	0.8%	1.6%	5.2%
	j=3	-5.6%	-4.8%	-3.9%
	j=4	-10.0%	-9.5%	-6.9%

Because the powder in the dispenser before printing contains a mixture of fine and larger particles, the recoater spreads more particles smaller than the layer thickness (40 µm) at the beginning of the powder bed (a_{14}, a_{24}, a_{34}, a_{44}), while coarser particles, bigger than 40 µm, are dragged further away. This result is also reported by Carrion *et al*. [24]. Moreover, Pal *et al*. [11] reported that the bulk density of the powder bed drops near the collector bin. It was also observed that near the dispenser, the D05, D50, and D10 values are slightly lower than those measured near the collector bin, whereas D90 and D95 showed an increase of 1.2 µm and 1.5 µm, respectively, near the dispenser [18]. However, the decrease in particle diameters along the columns remains unjustified and is not discussed in the literature.

3.2. Results of Experiment 2: Evolution of PSD depending on position relative to a printed part

3.2.1. Results of single contamination:

Figure 1-10 shows the locations of 6 powder samples collected along the horizontal x-axis, and 6 samples collected along the vertical y-axis. Figures 1-11 and 1-12 show that the cumulative PSD and the PSD of samples positioned in negative abscissas x_{-1}, x_{-2} , x_{-3} (near the collector bin) are greater than those located in the positive abscissas x_1, x_2, x_3 (near the dispenser), indicating the same result as the first experiment, which demonstrated that the PSD in the graph is displaced progressively left toward fine particles as the sample location moves rightward on the build plate. In addition, the diameter values D90, D50 and D10 decrease by 5.1%, 12.1%, and 18%, respectively, toward the positive abscissas (see Figure 1-13). Yet, the PSDs of samples taken on the y-axis are superposed, and their diameter values remain approximately stable (see Figure 1-14). As also shown in Figure 1-10, the powder bed area located below the printed cylinder shows a substantial amount of fine black particles as compared to the top area. The black particles are most likely spatters generated during printing of the solid cylinder and carried by the inert gas flowing from the top of the build

plate toward the bottom [12]. However, their impact on powder size along the y-axis is negligible. Figure 1-10 also shows that spatters are not visible in the powder bed along the x-axis. Changes to the PSD along this axis are comparable to the recoater effect identified in the first experiment.

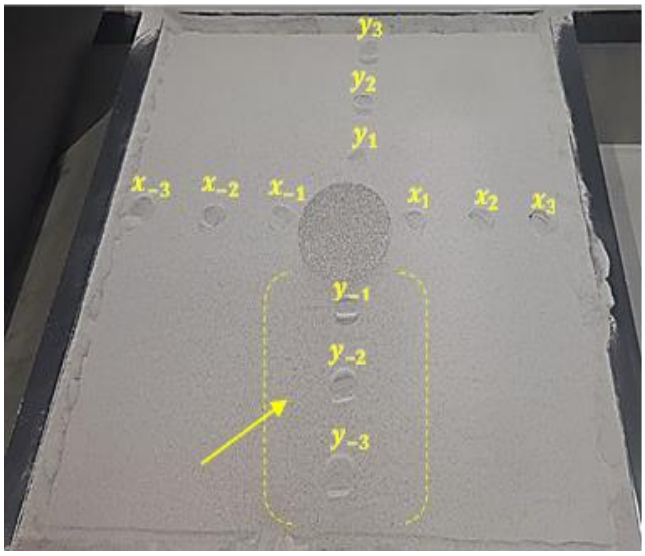

Figure 1-10: Location of powder samples collected along horizontal x-axis and vertical y-axis

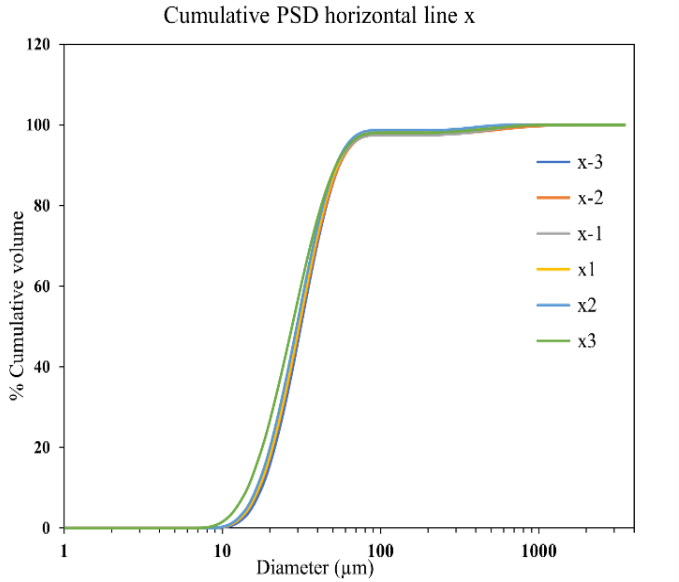

Figure 1-11: Cumulative PSD horizontal line

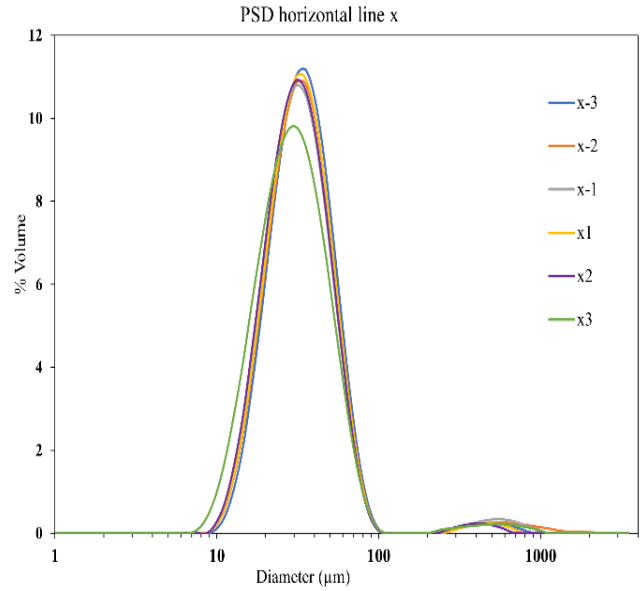

Figure 1-12: PSD horizontal line

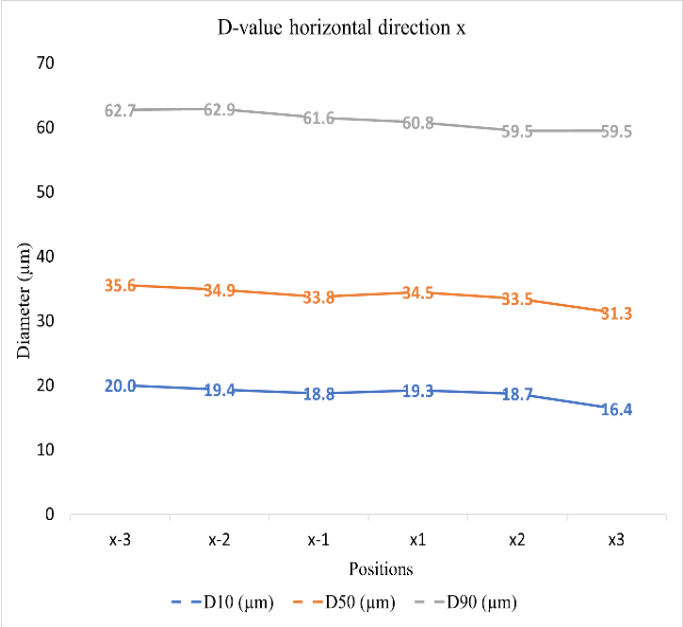

Figure 1-13: D-value horizontal line (x-axis)

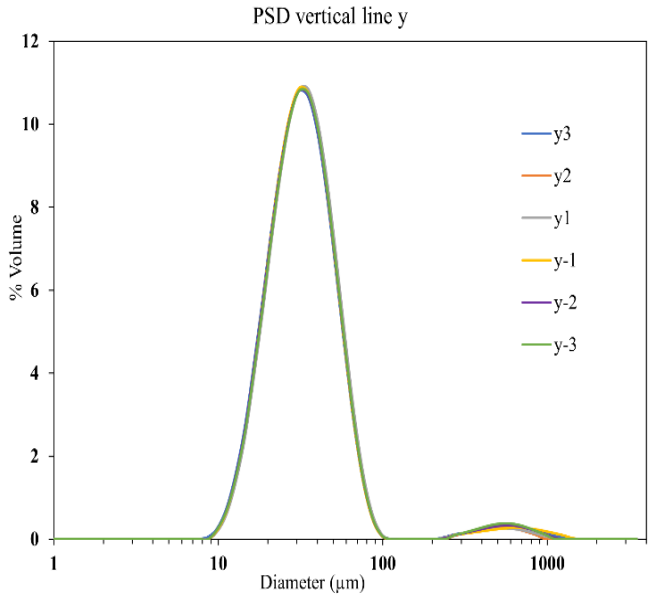

Figure 1-14: PSD vertical line

3.2.2. Results of double contamination

Figure 1-15 illustrates the four concentric cylinders printed for Experiment 2B to study what happens when parts are printed in close proximity. As can be seen in Figure 1-16, the cumulative PSD shifts gradually rightward toward bigger particles, followed by a significant drop in the proportion of fine particles with the gradual movement from zone 4 to zone 1. This implies that zone 1 includes more coarse particles and less fine particles than zones 2, 3, or 4.

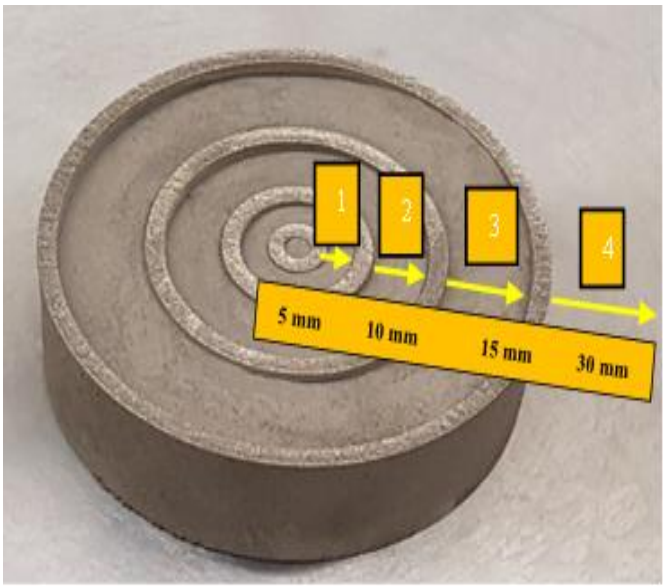

Figure 1-15: Part with four concentric cylinders with increasing distance of spacing

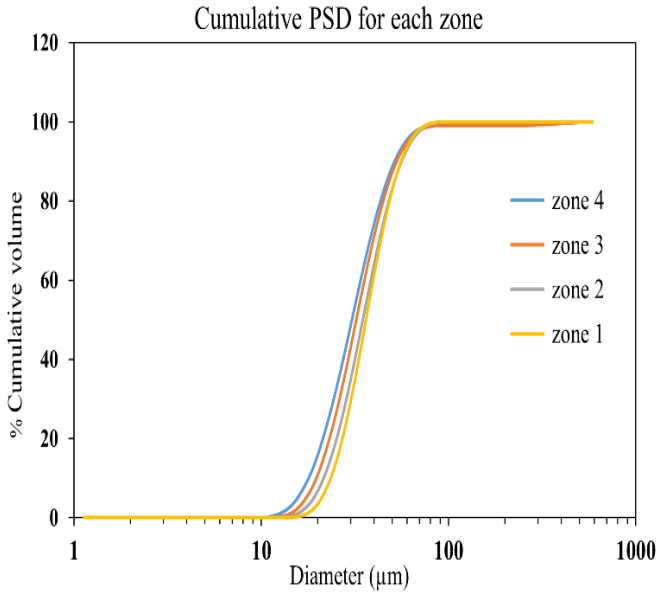

Figure 1-16: Cumulative PSD measured for each zone

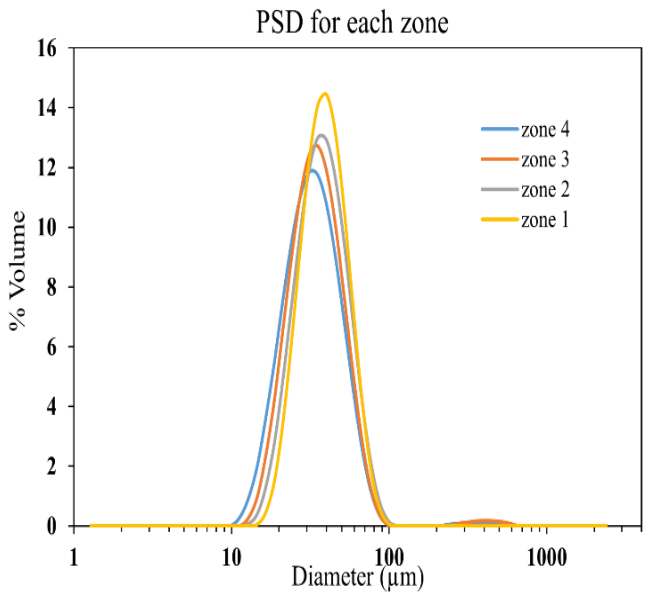

Figure 1-17: PSD measured for each zone

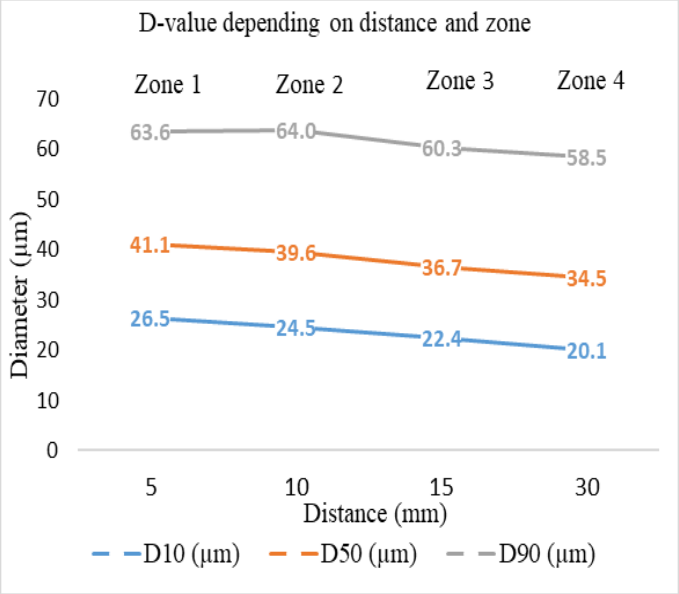

Figure 1-18: D-value depending on distance spacing and zone

Figure 1-17 shows that the PSD moved rightward and become narrower from zone 4 to zone 1. Likewise, the percentage of smaller particles is significantly reduced. As we can see in Figure 1-18, the particle diameters D90, D50, and D10 increase gradually by 8%, 16% and 24%, respectively, as we move from zone 4 to zone 1. As can be observed in this experiment, reducing the distance between melted parts increases the proportion of coarse particles and significantly reduces the percentage of fine particles in the area. Powder located at a distance from the melt pool remains unaffected, with a PSD quite similar to that measured in the dispenser.

This change could be attributed to the fact that laser melting creates spatters and larger particles. This condensation occurs due to the vaporization of melted particles [6, 18]. Furthermore, they may agglomerate into bigger particles to create satellites. Soundarapandiyan *et al*. [22] reported that powder particles located near the melt zone are not only coarser with a wider PSD than particles away from the melt pool, but they also demonstrate a dramatic degradation in their morphology: partial melting, hard sintering, and agglomerations. The results of this experiment are also confirmed by Sutton *et al*. [15] who concluded that heat affects particles located near the melt pool (zone 1). Consequently, heat-

affected particles become irregular in shape and coarser than particle coming from unused powder. Recent studies [15, 22, 37, 41, 42] on the effects of reusing powder show that the PSD shifts rightward toward large particles after reuse cycles. In addition, the proportion of fine particles drops, whereas the proportion of bigger particles grows. Consequently, we can establish a similarity between the powder alteration caused by the proximity of printed parts and reuse cycles; the smaller the distance between printed parts, the more the powder is altered. Many authors [1, 6, 24, 40] claim that the reduction in fine particles minimizes agglomeration effects, which improves powder flowability. However, a decrease in the smallest particles and the presence of coarser particles may be responsible for an increase in the percentage of void within the powder bed, so that the printed part can be impacted by a lack of fusion [6, 22].

3.3. Results of Experiment 3: PSD changes when printing lattice structures of different cell sizes

Figure 1-4 shows the four lattice cylinders printed with varying cell sizes of 2 mm, 3 mm, 4 mm, and 5 mm. The powder samples are extracted from the lattices at the locations indicated by the yellow arrows. The PSD for the four different lattice cell sizes is not superposed, as can be seen in Figure 1-19. The PSD of powder trapped in the 2-mm-cell lattice shows a lower proportion of tiny particles and a slightly higher percentage of larger particles than the 5-mm-cell lattice. This finding is similar to the results of the second experiment, which reported a relevant decrease in small particles as the distance of spacing between parts was reduced.

As Figure 1-20 illustrates, the powder samples taken from the lattice structures show a significant proportion of particles with diameters d larger than 976 µm (~ 1 mm), which are not found in other PSDs. Increasing the lattice cell sizes from 2 to 5 mm increased the volume proportion of these large particles from 1.4% to 6.5%. Large particles were not detected in new powder nor in the dispenser. Changing the cell size of the lattice, as previously described in table 1-1, varied the area and volume ratios of the printed lattice cylinders. Figure 1-21

illustrates that increasing the area ratio from 2.4 to 8.4 raised the diameter D-values D10 and D50 by 16.2% and 9%, respectively, while D90 decreased by 13%.

When printing the lattice cylinders, the powder had already been recycled 11 times. Figure 1-22 illustrate the evolution of powder diameter values when comparing the diameter value of new powder with the diameter value of powder reused 12 times. Significant increases can be observed in D90, D50 and D10, of 21.7%, 16.6% and 15.5%, respectively. The PSD moves larger particles rightward, followed by a slight drop in fine particles and a relevant increase in the proportion of large particles (Figure 1-23). This result is also reported by many researchers studying the effects of reuse cycles on powder size characteristics [15, 20, 22, 24, 41-43].

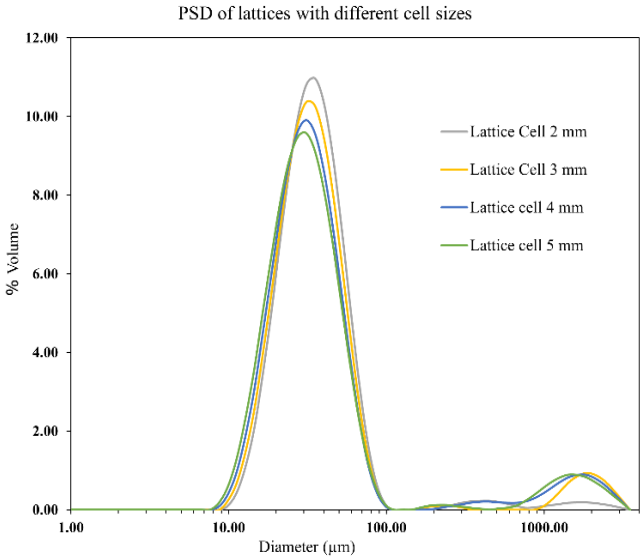

Figure 1-19: PSD of lattices parts with different cell sizes

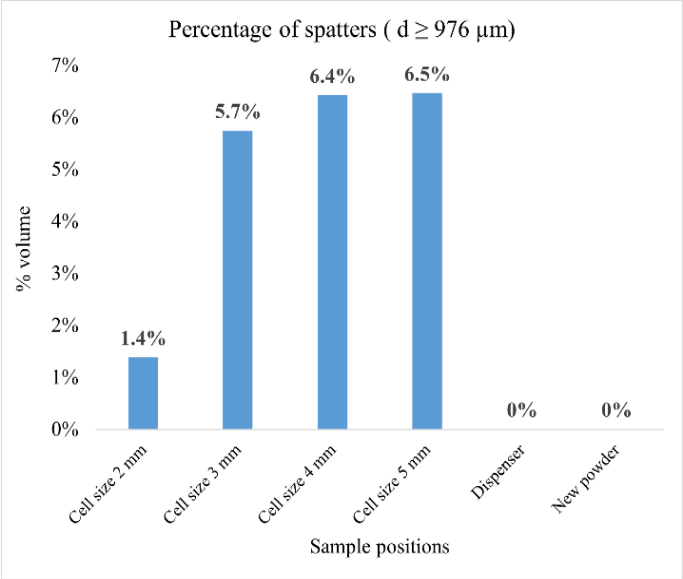

Figure 1-20: Percentage of larger particles (spatters) generated by lattices

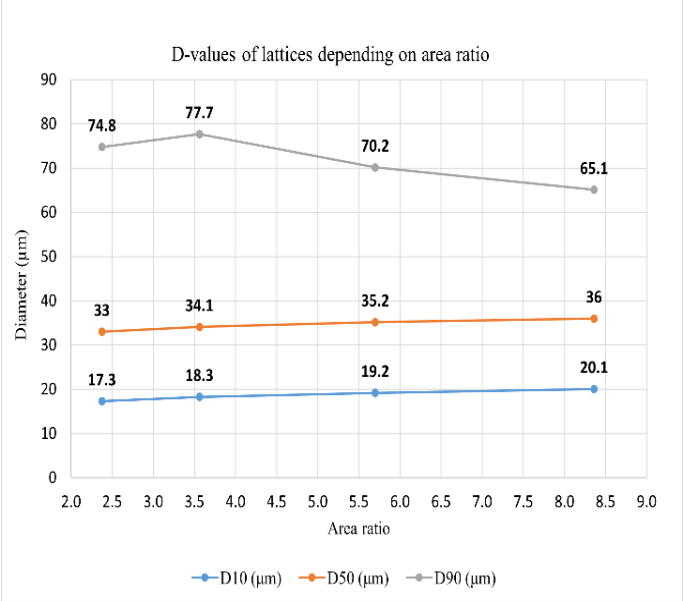

Figure 1-21: D-value of lattices parts depending on area ratio

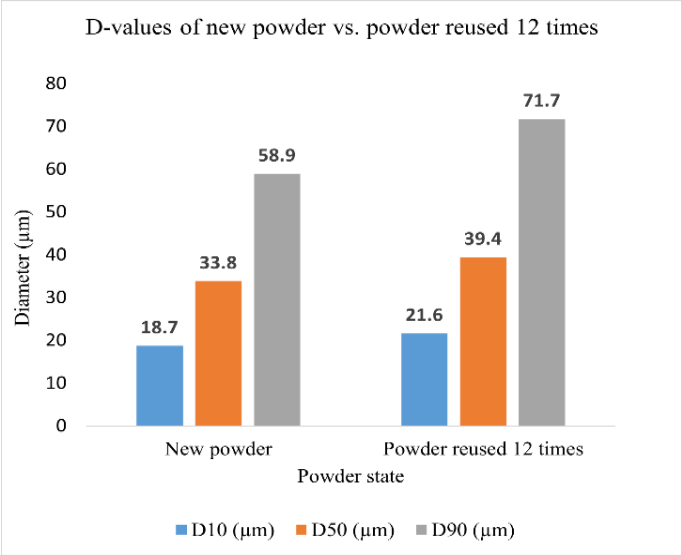

Figure 1-22: D-values of new powder versus powder reused 12 times

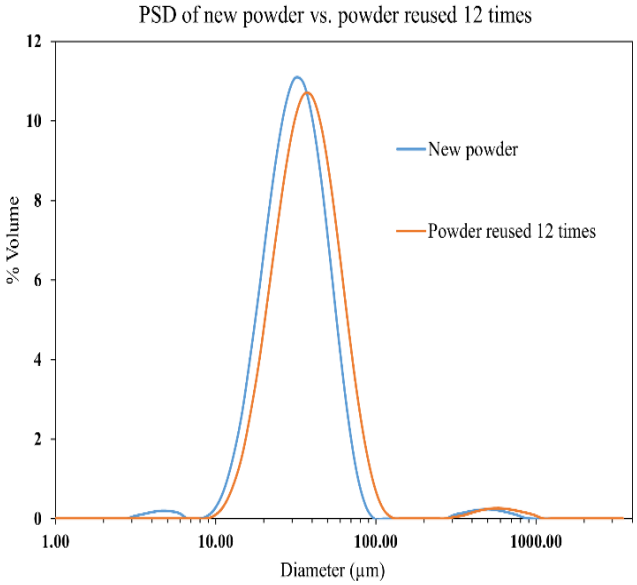

Figure 1-23: PSD of new powder versus powder reused 12 times

As previously discussed, Figure 1-21 shows that D-values D10 and D50 increased by 16.2% and 9% respectively, while the D90 decreased by 13% when the area ratio was increased from 2.4 to 8.4. As a result, it's possible to deduce that increasing the area and volume ratio of printed components in these lattice cylinders changes the PSD of the powder trapped in the lattice structure. This outcome might be due to a variety of circumstances. The balling defect might be responsible for the increase in powder diameter to 500 µm due to the creation of partially melted particles [17]. Furthermore, formation of spatters could be the primary reason for the increase in PSD. As shown in Figure 1-20, particles with diameters greater than 976 µm (~1 mm) were absent in samples taken in the dispenser and in the new powder, but they were present in samples taken from the powder trapped inside the four lattices. Sutton *et al*. [14] verified this assumption, reporting that heat-affected powder became coarser and had an irregular morphology owing to spatters. Furthermore, Gowtham *et al*. [22, 44] observed that powder near the melt pool was coarser due to the presence of spatters, partially melted particles, hard sintering, and agglomerations.

As can be noticed in figure 1-23, the PSD measurement show a very slight proportion of larger particles (0.73% for new powder and 1.19% for powder reused 12 times) which diameters are between 500-1000 µm. This small proportion of large particles were likely aggregates detected by Mastersizer 3000 but not present in powder samples observed using the electron microscope.

As can be noticed in Figure 1-24 the morphology of new powder is globally spherical with the presence of satellites and aggregates particles (indicated with red circles), which are formed during the powder production process. However, Figure 1-25 show that the powder recycled 12 times exhibits an important presence of satellites, deformed particles (indicated with orange circles), Clip-Clap (indicated with blue circles), and elongated particles (indicated with yellow circles). Furthermore, as it can be seen in Figure 1-26, the powder inside the 3-mm-cell lattice shows a high shape degradation. The particles are deformed and exhibit a relevant amount of aggregates, elongated particles, broken particles (indicated with green circles), and shattered particles (indicated with white circles). Lastly, Figure 1-27

shows spatters and heat-affected particles that were trapped within the 80-µm-mesh sieve device. The particles exhibit a considerable prevalence of aggregate particles in addition to the presence of spherical larger particles “Super ball” (indicated by purple circles).

Many researches have noticed the degradation of particles morphology after reusing cycles, especially the presence of defects such as broken particles, clip-clap, shattered particles, deformed particles, elongated particles, aggregates, and particles with molten specks. This powder alteration is attributed to the effect of melting and sintering process [18, 21, 22, 33, 44, 45].

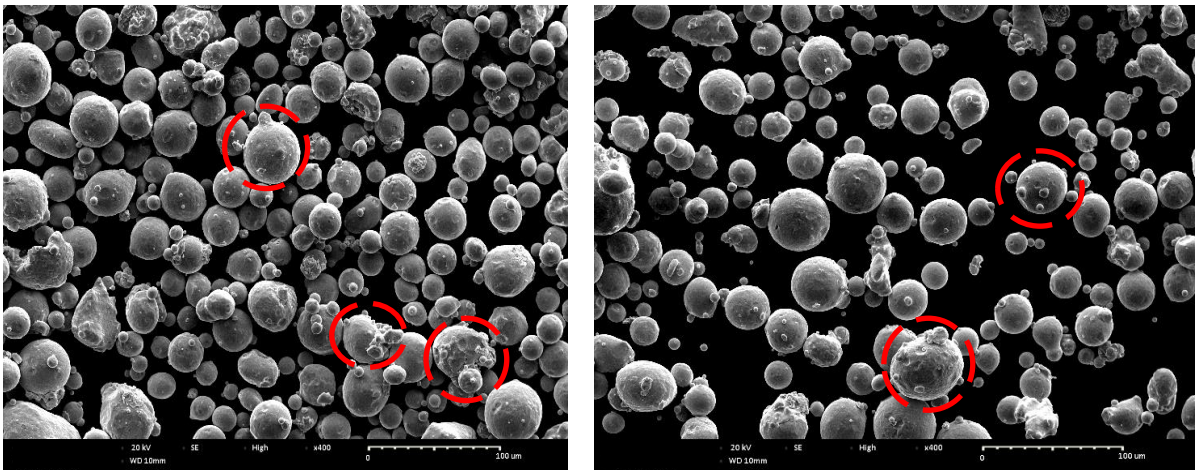

Figure 1-24: Morphologies of new powder

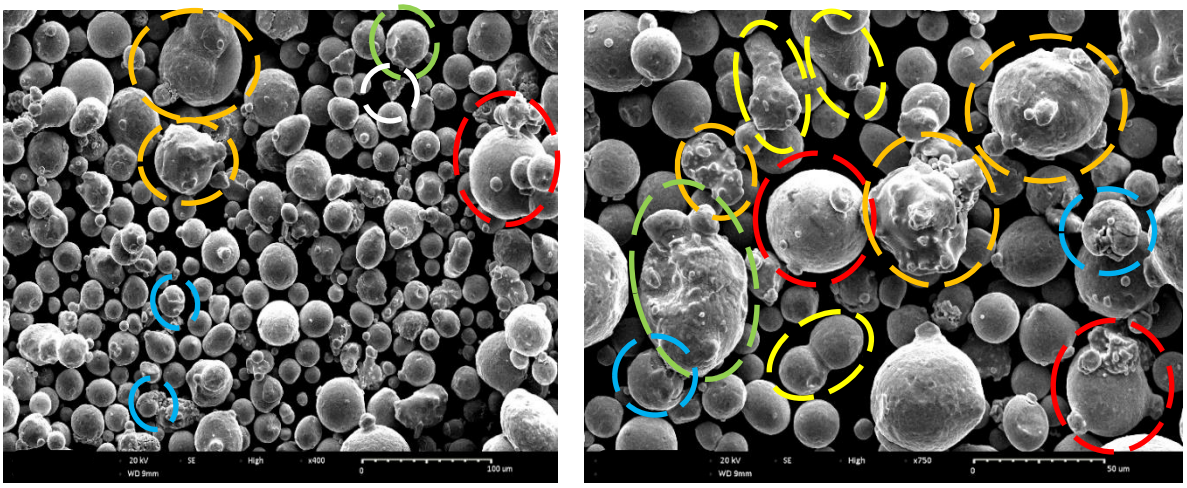

Figure 1-25: Morphologies of powder reused 12

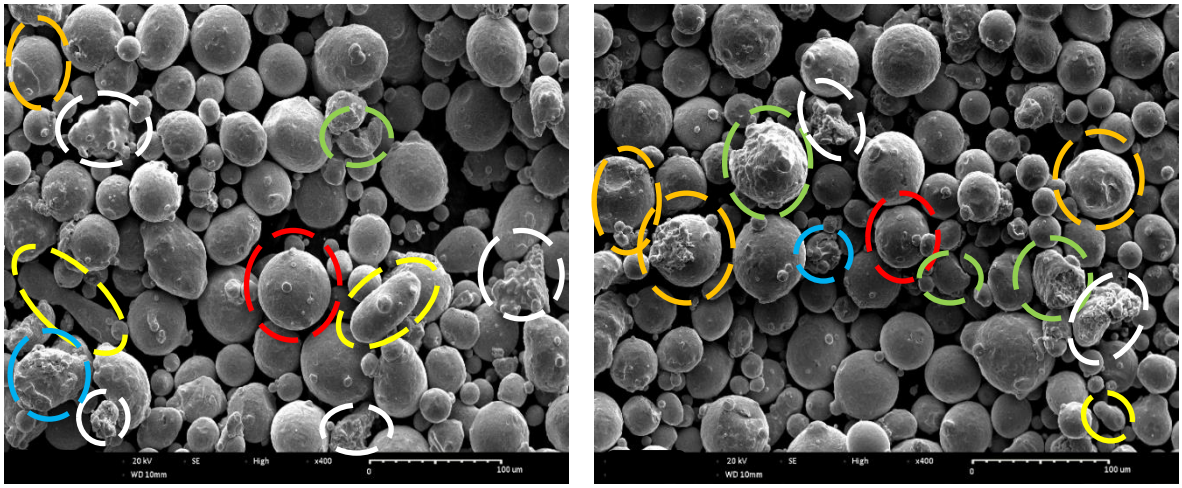

Figure 1-26: Powder confined inside 3-mm-cell lattice

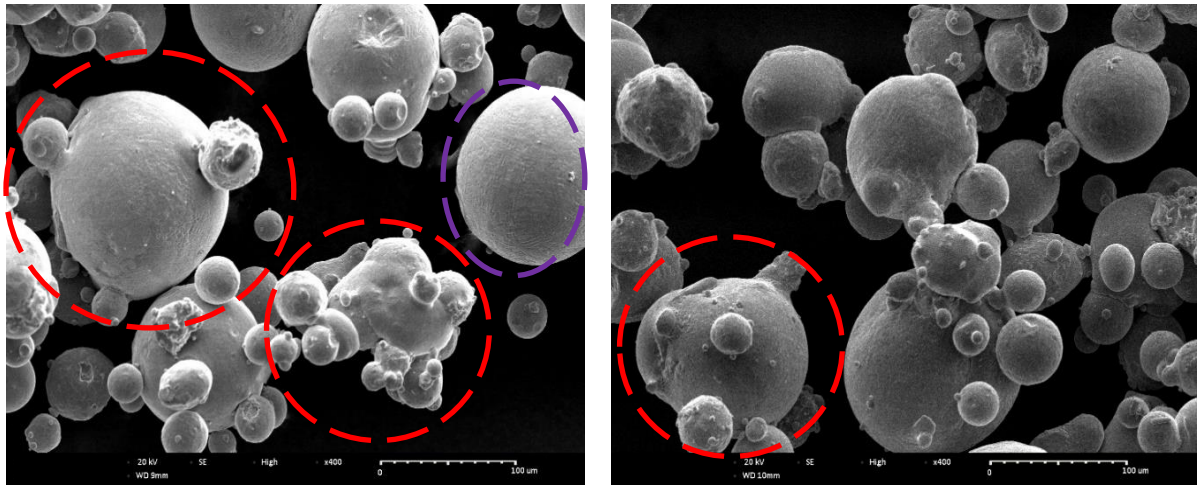

Figure 1-27: Heat-affected powder trapped in sieve

4. Conclusions:

The evolution of particle size distribution throughout the printing cycle and recycling of the L-PBF process were examined, as well as the influence of printed component geometry on powder size and morphology. The following conclusions may be drawn from the different experiments described above.

Experiment 1 examined how powder was spread on the bed. The results showed that the powder is not uniformly spread over the build plate. Therefore, the PSD changed more along horizontal lines than along vertical lines, due to the recoater effect and powder flowability. When moving horizontally toward the collector, the diameter D-values D90, D50, and D10 progressively increased. For example, the D50 increased by 9.8%, 10.8%, 9.6%, and 14.6% for the four different lines. However, moving from the top to the bottom of the powder bed through the vertical columns j = 1, 2, 3, 4, the diameters D-values mildly reduced. Moreover, the PSD of the sieved and recycled powders slowly changed during one printing cycle.

In Experiment 2A, a filled cylinder in the middle of the build plate was printed. The printing process produced spatters which were deposited in the inferior region of the powder bed due to the effect of gas flow, but their influence on PSD along the vertical axis (y-axis) was negligible. Nevertheless, the powder samples obtained along the horizontal line (x-axis) showed an increase in PSD in the direction of the recoater, as measured in Experiment 1. In Experiment 2B, we examined the influence of part distance spacing on PSD. We can conclude that decreasing the spacing between parts narrows and shifts the PSD toward larger particles.

Finally, in Experiment 3, a printing situation with significant potential for powder alteration was explored. Lattice structures of different cell sizes were printed, then the PSD and the morphology of the powder trapped in the lattices were analyzed. The PSD was quite different and coarse particles with diameters above approximately 1 mm were detected during powder analysis. Moreover, they were not detected after sieving. These could be attributed solely to spatters and agglomerate particles formed in the powder stuck inside the lattice cylinders. This powder morphology was dramatically impacted duo to the formation of aggregates, elongated, broken, ‘‘Clip-Clap’’ and shattered particles.

From these results, it’s possible to confirm the degradation and alteration of the powder bed PSD and morphology due to the printing process generating spatters and particle agglomerations. After significant courses of recycling, the PSD of the powder showed more coarse particles and less fine particles, as well as a relevant increase in the proportion of large particles and significant presence of aggregates, deformed and elongated particles within the recycled powder.

CHAPITRE 2
EFFET DU RECYCLAGE DE LA POUDRE D'ACIER MARAGING SUR LE COMPORTEMENT EN TRACTION ET EN FATIGUE DES PIÈCES FABRIQUÉES PAR LE PROCÉDÉ DE FUSION DE POUDRE PAR LASER

2.1 RÉSUMÉ EN FRANÇAIS DU DEUXIÈME ARTICLE

Le recyclage de la poudre est indispensable pour garantir la rentabilité du procédé de fusion par laser (laser-powder bed fusion : L-PBF). Cependant, les propriétés de la poudre recyclée peuvent varier après chaque cycle d'impression et la procédure de validation de la qualité de la poudre est difficile à mettre en place. Malgré toutes les études publiées jusqu'à maintenant, il demeure difficile de garantir les performances mécaniques des pièces imprimées à partir d'une poudre réutilisées plusieurs fois. Par conséquent les fabricants préfèrent utiliser une poudre neuve pour imprimer des composants qui jouent un rôle critique, ce qui augmente significativement le coût de fabrication. En s'appuyant sur les résultats présentés dans l'article 1 du présent mémoire et en s'inspirant de plusieurs autres études [11, 12, 15, 16, 25, 46] il a été démontré que la poudre subit une altération et que ses caractéristiques dépendent de plusieurs facteurs : le type de matériau, les paramètres d'impression, la géométrie des pièces, le nombre de recyclage, et les techniques de stockage et de tamisage de la poudre. C'est pourquoi cet article vise à investiguer l'effet de recyclage sur les caractéristiques de la poudre an acier maraging et sur les propriétés statiques et le comportement en fatigue des pièces imprimées à partir de cette poudre. Pour cela, on a effectué huit impressions, chacune contenant 4 éprouvettes de traction et 17 éprouvettes de fatigue, ainsi que 4 cylindres en structure treillis. Après chaque impression la hauteur du volume d'impression a été réduite dans le but de compenser la quantité de poudre consommée et éviter d'ajouter la poudre neuve. Durant chaque cycle, la poudre non fusionnée a été tamisée, la densité apparente a été mesurée, le PSD a été analyser et la morphologie des particules a été observée avant l'impression suivante.

Finalement, des tests de traction et de fatigue ont été réalisés sur les éprouvettes. Ces tests ont permis d'évaluer les propriétés de la poudre et la variation des caractéristiques mécaniques de traction et de fatigue des pièces imprimées après 8 cycles. Cette évaluation a permis de faire plusieurs constatations. La

densité apparente de la poudre est restée stable autour de 4,64 g/ml après chaque cycle d'impression. Le PSD s'est déplacé à droite vers les particules les plus grosses après 8 cycles indiquant une augmentation de la proportion des grosses particules et une légère diminution de des particules fines. Par ailleurs, la morphologie de la poudre est considérablement altérée. En effet, la poudre recyclée 8 fois comporte une quantité importante d'agrégats, de particules allongées et déformées. La rugosité de surface des pièces brutes est restée quasiment stable avec une valeur Ra moyenne de 8,22 µm. Les propriétés mécaniques en traction n'ont pas subi de grands changements après le recyclage. La résistance à la traction a diminué de 3. 6%, passant de 1985 MPa à 1913 MPa. De son côté, la limite d'élasticité (0,2% YS) a également baissé de 3%, passant de 1917 MPa à 1859 MPa. Le module de Young a été diminué de 2,6%, passant de 189 GPa à 184 GPa et la déformation à la rupture est restée stable à 1,58 %. La limite d'endurance obtenue par la méthode de l'escalier est restée constante malgré une légère diminution de 2,7 % , passant de 332 à 323 MPa. Si en moyenne les propriétés mécaniques ont très peu changé, l'écart type a diminué significativement, passant de 41 à 10,6 MPa après huit impressions. L'observation des faciès de rupture a démontré que les pièces issues de la poudre recyclée 8 fois présentent davantage de porosités, de manque de fusion, de particules partiellement fusionnées et d'inclusions métalliques et carboniques.

Cet article, intitulé « Maraging Steel Powder Recycling Effect on the Tensile and Fatigue Behavior of Parts Produced Through the Laser Powder Bed Fusion (L-PBF) Process», a été soumis le 22/11/2022 au journal *The Iternational Journal of Advanced Manufacturing Technology*. En tant que premier auteur, j'ai contribué à l'essentiel de la recherche sur l'état de la question, au développement de la méthode et à l'exécution des travaux expérimentaux. Le professeur Jean Brousseau, second auteur, a fourni l'idée originale, a aidé à la recherche sur l'état de la question, a contribué au développement de la méthode ainsi qu'à la révision de l'article. M. Claude Belzile a participé à l'exécution des tests d'analyse des propriétés de la poudre et M. Abderrazak El Ouafi a contribué à la planification des expériences et à la révision de l'article.

2.2 EFFET DU RECYCLAGE DE LA POUDRE D'ACIER MARAGING SUR LES PROPRIÉTÉS EN TRACTION ET EN FATIGUE DES PIÈCES FABRIQUÉES PAR LE PROCÉDÉ DE FUSION DE POUDRE PAR LASER (L-PBF)

Maraging Steel Powder Recycling Effect on the Tensile and Fatigue Behavior of Parts Produced Through the Laser Powder Bed Fusion (L-PBF) Process

Othmane Rayan,[a] Jean Brousseau,[a] Claude Belzile,[b] Abderrazak El Ouafi[a]

[a] Department of Mathematics, Computer Science and Engineering, Université du Québec à Rimouski (UQAR), 300, allée des Ursulines, C.P. 3300, Rimouski, QC G5L 3A1, Canada.
[b] Institut des sciences de la mer de Rimouski (ISMER), Université du Québec à Rimouski, 310 allée des Ursulines, Rimouski, QC, G5L 3A1, Canada.

ABSTRACT

Additive manufacturing (AM) has advanced the manufacturing industry and has been employed in a wide range of industrial applications, including in aerospace, automotive, medical and die-casting equipment. To ensure the cost-effectiveness of the AM process, unfused powder must be recycled even if its characteristics may change after each cycle, making essential the validation of powder quality and component mechanical performances. Despite the research published to date, predicting the mechanical performance of printed parts issued from reused powder remains challenging since it is dependent on many AM process variables. Until now, no research has looked at the impact of powder recycling on the fatigue behavior of maraging steel components. This study investigates the impact of maraging steel powder reuse on powder characteristics, as well as on the tensile and fatigue properties of printed components. Our results indicate that the powder particle size distribution increased after eight powder recycling, particle morphology showed the presence of aggregates, broken particles, shattered and deformed particles, while powder apparent density remained constant. Powder reusing had no significant impact on the surface roughness of as-built specimens. Although there was a slight decrease in mechanical properties over reuse cycles, tensile and fatigue performance remained globally stable, while the standard deviation of fatigue stress became narrower after eight cycles. Finally, fractography revealed that the

fatigue fracture surfaces of components manufactured from an eight-time recycled powder have more fusion defects and carbon inclusions than the parts made from virgin powder.

1. Introduction

There has been a growing interest in metallic additive manufacturing (AM) due to the multiple benefits of printing sophisticated products that are light weight and offer high accuracy, near-net-shape features and excellent mechanical performance [1]. Among the most prevalent metallic additive manufacturing processes are Laser Powder Bed Fusion (L-PBF) and Electron Beam Melting (EBM). Both technologies use the same manufacturing process: a recoater device spreads a fine layer of powder over a substrate, then an energy source (a laser in the case of L-PBF, and an electron beam in the case of EBM) melts the powder layer by layer until the 3D part is formed. These processes make it possible to manufacture complex geometrical pieces with great dimension precision.

A drawback of L-PBF technology is the need to fill a larger volume than the volume of the printed parts. The unfused powder is exposed to different phenomena: a laser heat effect, a mechanical spreading process, a sieving process and a storage process. Thus, its chemical and physical properties are altered, which could also affect the mechanical properties of the manufactured components. Because metallic powder is costly, unfused powder should be sieved and prepared for subsequent prints to ensure that the additive manufacturing process is cost efficient. In a case study, LPW Technology Ltd claimed a 92% decrease in material costs when powder was reused 15 times (Rushton, 2019) [8]. Moreover, the new technology of plasma spheroidization allows for recovery of reused powder, which makes AM a green and clean process [8].

Recycling is necessary to keep costs as low as possible and to minimize the environmental impact. Although many studies have been conducted to date, the issue of how recycling powder impacts its chemical and physical features, and the mechanical behavior of the printed component is still not completely understood [13]. Thus, engineers are still unsure about the performance of printed parts made from recycled powder, particularly when it comes to critical components [33]. According to recent studies [1, 23], the spherical shape is the most appropriate shape for metal AM because it enhances powder flowability. The spherical shape also boosts other mechanical characteristics, notably ultimate tensile strength and yield strength, as well as surface roughness and dimension accuracy. Moreover, Bochuan Liu

et al. [47] have noted that wide particle size distribution (PSD) delivers superior powder bed density, parts with higher density and smoother surface finish while powder with a narrower PSD has higher flowability and creates components with ideal tensile properties and hardness.

It is recognized that printing and sieving processes affect the chemical composition of the powder. Many researchers have reported a change in powder composition, especially the percentage of oxygen content. Tang *et al*. [36] observed a progressive increase in the oxygen content in the composition of Ti 6Al 4V, from 0.08% to 0.19%, after 21 reuses. Consequently, ultimate strength and yield strength increased by 13% and 15%, respectively. In addition to the influence of the process, chemical composition can also be affected by storage techniques. Indeed, when the powder is not stored under inert gas, it is very susceptible to contamination by ambient air, which carries pollutants, fibers and dust, and can also be influenced by humidity, corrosion and oxidation [8]. Furthermore, Moghimian *et al*. [13] presented an overview of the factors affecting both the powder quality and the mechanical properties of different materials: powder production methods, L-PBF printing parameters, powder recycling, powder blending and the sieving process.

Several researchers have recently studied the effect of reusing powder on chemical and physical powder characteristics and the mechanical performance of components produced with L-PBF and EBM technologies for different materials, such as titanium Ti-6Al-4V [9, 17, 22, 24, 33, 34, 37, 43], stainless steel [25, 38, 41, 45, 48], aluminum AlSi10Mg [16, 49], Inconel 718 [20, 35, 42] and maraging steel [14]. The following paragraphs summarize the information relative to each of these alloys.

Titanium Ti-6Al-4V material

Carrion *et al*. [24] evaluated the powder properties and mechanical properties of Ti-6Al-4V L-PBF specimens. After 15 reusing cycles, the particle size distribution became narrower, and the particles' diameter value D90 decreased by 18.7%. The powder flowability was improved significantly. The particles' morphology was not greatly modified. Furthermore, they observed that recycling had no effect on the tensile and fatigue behavior of specimens in the as-built surface state. However, when they machined the specimens made from used powder, the fatigue behavior in the high cycle regime of the specimen printed from recycled powder improved when compared with specimens made from new powder.

According to Quintana *et al*. [17], the particle size of the powder bed and the dispenser powder decreased with the number of reuses, and their shapes remained mostly spherical. Flowability was

improved, while tap density decreased slightly as the number of reuses increased. A small increase in tensile strength was noted after 31 build cycles owing to the increased oxygen content.

However, Renishaw plc (2016) [34] noted that Ti-6Al-4V powder PSD increased and became tighter, which improved flowability. Particle morphology remained mostly spherical over 38 cycles, with the occasional presence of aggregates and elongated particles. The ultimate tensile strength (UTS) and yield strength (0.2% YS) values increased slightly, by 100 MPa and 128 MPa, respectively, from virgin to build 38. These changes may be attributable to an increase in oxygen and nitrogen levels. The strain at break stayed almost constant.

Moreover, O'Leary [37] detected an increase in titanium particle size distribution (PSD), with a decrease in the number of smaller particles less than 15 µm and an increase in the number of larger particles greater than 45 µm, after five reuse cycles. Reused powder surfaces were rougher and less spherical. Like O'Leary, Seyda *et al*. [43] noted an increase in the PSD of L-PBF Ti-6Al-4V powder and an improvement in apparent density and flowability after 12 recycling iterations. However, the surface roughness of printed parts was drastically impacted. That said, the parts produced from reused powder exhibited better hardness and tensile strength than specimens fabricated from virgin powder. According to the authors, the improvements were related to the increase in powder density and the presence of oxygen in the melt pool carried by the ambient atmosphere during the powder sieving process.

Additionally, Soundarapandiyan *et al*. [22] observed that particle size distribution increased and became wider on region near the melt pool because particles were partially melted, hard-sintered and agglomerated. Away from the melt zone, the PSD was narrower, and particle shape remained almost spherical. After 10 reuse cycles, the PSD moved slightly to the coarser side, the powder sphericity rose by 26% over the sphericity of fresh powder, and the number of satellites and finer particles decreased, resulting in enhanced flowability and density. The microstructure, Charpy impact energy, hardness and elongation parameters did not change significantly. Because of the modest rise in recycled powder oxygen concentration, yield strength and tensile strength increased slightly. The fatigue life of recycled components was reduced due to an increase in lack of fusion defects and porosity.

In their study, Alamos *et al*. [9] concluded that there was no substantial change in the mechanical tensile properties of L-PBF Ti-6Al-4V after eight reuse cycles. PSD narrowed slightly, but the diameter values D90, D50 and D10 were almost unchanged. The density of the printed components remained consistent.

Moreover, Popov *et al*.[33] reported that after 69 reuse cycles in EBM machines, the Ti-6Al-4V particles were significantly damaged by the laser heat exposure and sieving process during powder recycling. The powder particle shapes were altered by the formation of elongated, "clip-clap" particles, agglomerates and broken particles. After the reuse cycles, UTS and YS rose slightly, while the elongation of the samples was significantly decreased. Samples produced from reused powder have exhibited a much lower fatigue life because of the existence of porosity, partially melted particles, and lack of fusion defects. However, the hot isostatic pressing (HIP) treatment enhanced fatigue life of specimens built from recycled powder.

Stainless steel material

Contaldi *et al*. [41] investigated the effect of powder reuse on two types of precipitation hardening stainless steel, the martensitic PH1 and the austenitic GP1. The PSD for both materials became narrower and showed a slight decrease of small particles over nine reuses. After recycling, the presence of oval-shaped particles and agglomeration in both materials differed from the normal spherical particle form. Furthermore, chemical composition, tap density, and apparent density of both materials remained relatively stable. The mechanical characteristics of PH1 were found to be insensitive to powder reuse, with only the elongation at break being slightly affected. However, samples printed from GP1 powder were more impacted, particularly yield strength, which rose by 190 MPa, and elongation at break, which decreased by 6%. The fatigue behavior of both materials remained generally constant over nine reuse cycles.

Ahmed *et al*. [45] noted a minor increase in the 17-4 PH stainless steel PSD over 10 reuse cycles. As irregular shaped particles grew in the feedstock, powder's flowability decreased. When compared with the first sample, the tenth specimen showed a 54% increase in pore size and a 17% increase in surface roughness, which led to a 7% drop in ductility. The UTS was not substantially changed.

Indeed, Arash Soltani-Tehrani *et al*. [25] remarked that the 17-4 PH stainless steel powder PSD got slightly narrower and shifted to the left, indicating a drop in the fraction of larger particles and a decrease in the proportion of fine particles (smaller than 15 μm) after 14 reuse cycles. Most of the particles remained spherical, which improved flowability. The researchers also observed that recycling and component location on the building plate had no influence on the tensile and fatigue behavior of specimens in their as-built surface condition. However, after machining the specimens built from recycled powder, their

fatigue behavior in the high cycle regime improved remarkably, especially for the specimens located further away from the dispenser.

According to Jacob *et al*. [48], the hardness of the 17-4 PH stainless steel parts, tensile strength and surface roughness showed no change throughout 11 reuse cycles. The recycled powder showed no change in either particle size distribution (PSD) or particle shape, while apparent and packed densities increased and flowability improved.

Moreover, Sutton *et al*.[38] reported that laser spatters, known as ejecta, compromised the morphological and chemical properties of AISI 304L stainless steel reused powder. After five cycles, the powder particles were coarser and their shapes became irregular. Powder-bed density showed a substantial increase since powder flowability was improved over reuse cycles. Tensile properties were marginally influenced throughout reuse cycles, which was linked to the existence of large pores on fracture surfaces. Additionally, it was noted that there was a declining trend in Charpy impact toughness due to the rise in oxygen content during printing iteration.

Aluminum alloy AlSi10Mg material

Del Re *et al*. [16] investigated on a L-PBF printer the effect of recycling AlSi10Mg powder on its physical and chemical properties as well as on the mechanical properties of printed parts. After eight reuse cycles, they discovered that particles shape was less spherical with the presence of agglomerate particles. Furthermore, the PSD of the reused powder showed a slight leftward shift toward fine particles, indicating a progressive decrease of coarser particle content owing to the sieving operation. Over the eight reuse cycles, apparent and tap densities and chemical composition stayed almost constant. However, yield and tensile strength declined by 10 MPa, while high cycle fatigue strength decreased from 160 to 145 MPa.

Asgari *et al*. [49] conducted a similar study for AlSi10Mg 200C parts. They concluded that the average particle size, microstructure, morphology and composition of the virgin and recycled powder were nearly identical. They differed only because of the presence of spatters, which showed an irregular shape, satellite particles, and rough powder particle surfaces. After printing cycles, there was no substantial change on the tensile properties of components.

Inconel 718 material

Yi *et al*. [20] reported that the Inconel 718 powder PSD increased, and particle morphology remained almost spherical after 14 reuse cycles. Furthermore, apparent density and flowability was significantly improved. There was a slight effect on the tensile properties of printed parts. Indeed, the UTS and YS stayed fairly constant, around 1025 MPa and 750 MPa, respectively, and the strain ranged from 27% to 30%.

Moreover, Rock *et al*. [35] studied the evolution of the physical and chemical characteristics of Inconel 718 powder after 10 building cycles. They observed that the PSD increased, the morphology of the particles was affected by the formation of agglomerates, and spatters with dendritic surfaces. Therefore, flowability significantly decreased after reusing.

Furthermore, Ardila *et al*. [42] analyzed the same material in an L-PBF machine and concluded that powder characteristics and mechanicals parts performance did not significantly change after 14 cycles. Most particles remained spherical, with a slight increase in size distribution. Microstructure and porosity were very similar in all iterations thanks to their recycling strategy, which consisted of sieving the unfused powder to eliminate aggregation and drying it in the oven with air circulation to remove humidity. For mechanical characteristics, they applied the Charpy test to specimens and remarked that toughness was almost unchanged after printing cycles.

Maraging steel MS1 material

Sun *et al*. [14] evaluated the powder characteristics and mechanical behavior of components fabricated from virgin and 113-time recycled maraging steel powder. They observed that there was no significant change in PSD and particle shape throughout reuse cycles. However, spatter particles caused oxide inclusion on the top surfaces of printed parts. They also discovered that as-built specimens created from 113-time recycled powder had nearly identical microstructure and mechanical properties to those produced from new powder (940 MPa yield strength, 1127 MPa ultimate tensile strength, 11% elongation, and 47.5 J impact fracture toughness at room temperature).

Similarly, to investigate the effect of powder contamination on the mechanical properties of 18Ni-300 maraging steel components, Gatto *et al*. [50] printed specimens from two separate batches. Batch 1 had a cross-contaminated raw powder that contained Ti-Al oxides, whereas batch 2 contained virgin maraging powder. They discovered that the presence of contaminants had no effect on static tensile characteristics.

However, fatigue endurance was dramatically compromised by contaminants (batch 1), while parts printed from clean powder (batch 2) had a fatigue life equivalent to forged specimens.

Finally, Horn *et al*. [51] discovered the presence of copper alloy CW106C foreign particles in the maraging steel powder feed stock, which happens during material changes inside the L-PBF machine or when using L-PBF multi-material machine. This cross-contamination decreased the parts' tensile properties and initiated cracks failure if the proportion of CW106C exceeded 2%.

The abovementioned research reveals that, overall, powder reuse improves powder density and flowability, with a slight change in powder size and morphology. The parts' tensile properties remain generally constant, but fatigue performance is negatively impacted by powder reuse. Consequently, the physical and chemical powder characteristics evolve inevitably, although slowly, when the powder passes multiple times through the printing and sieving process, which could also influence the mechanical properties of the final part. However, powder behavior differs from one material to another, because each material has its specific chemical and physical properties and materials react differently to additive manufacturing, especially to the recycling process.

Despite all of the studies published to date, the impact of recycling on powder properties and on static and fatigue behavior remains unclear and ambiguous. Very few studies have addressed the subject, especially with respect to maraging steel powder. This paper aims to investigate the effect of powder recycling on particle size distribution (PSD), particle morphology, powder apparent density, and the tensile and fatigue properties of maraging steel parts. We also conducted a fractography study to observe the fracture surface and investigate the causes of parts failure. Through this research, an effort is made to link the mechanical testing results and changes in powder properties by applying a precise experimental methodology and by monitoring the important variables.

2 EXPERIMENTAL METHODOLOGY

2.1 Material and powder characterization

The powder used was the EOS Maraging Steel MS1 (18% Ni Maraging 300). Its composition is detailed in Table 1 according to the material data sheet (EOS art-no.9011-0016) [3]. The study started with 20 kg

of fresh powder. The quantity was chosen to allow eight printing cycles and all the specimens needed to reach the end of the experiments within optimal time and cost efficiency. The methodology was inspired from many of the above-mentioned articles [9, 10, 16, 17, 35, 42, 52]. After each cycle, all unfused powder was sieved manually with an 80 µm sieve.

The powder samples were analyzed with a Malvern Panalytical Mastersizer 3000 particle-size analyzer equipped with a Hydro LV module following Rayan *et al* (submitted). The stirrer speed was set to 3000 rpm, a speed sufficient to keep the particles in suspension. Prior to the measurements, the sample was submitted for 60 s to Hydro LV ultrasounds at 25% power to help disintegrate aggregates. Three consecutive measurements of 30 s each were collected for each sample. The average statistics of the three measurements were computed (the coefficient of variation in Dv10, Dv50 and Dv90 of the three measurements was always <1%, indicating a good sample dispersion). The Mastersizer general purpose optical model for nonspherical particles was employed with a refractive index of 2.757 and absorption 1.0 for stainless steel (values taken from the Malvern Panalytical database included with Mastersizer 3000 software). Instrument performance was confirmed using Malvern Panalytical's QAS4002 Quality Audit Standard. Powder morphology was analyzed using a NanoImage SNE 4500M scanning electron microscope (SEM). Apparent powder density was measured with an electronic balance and 25-ml plastic graduated cylinder.

Table 2-1 The chemical composition MS1 virgin powder (in weight %) [4]

Element	Fe	Ni	Co	Mo	Ti	Al	Cr	Cu	C	Mn	Si	P	S
Max (%)	Balance	19	9.5	5.2	0.8	0.15	0.5	0.5	0.03	0.1	0.1	0.01	0.01
Min (%)		17	8.5	4.5	0.6	0.05	_	_	_	_	_	_	_

2.2 Machine/printing parameters

The parts were printed on an EOS M290 400W machine in a nitrogen atmosphere with less than 1.3% oxygen concentration and a chamber temperature of 40°C. The MS1 040 performance M291 2.00 EOSPRINT template was used: beam offset = 20 µm, building speed = 4.2 mm^3/s, layer thickness = 40

µm, hatch offset = 6 µm, and laser pattern = stripes rotated at a 47º angle with a 30º restriction angle at each next layer.

2.3 Recycling methodology

As in many other studies, for the recycling methodology we employed collective aging strategies to simulate the worst-case scenario of powder reuse [9, 10, 16, 18, 35, 42, 52]. Indeed, our recycling approach maximized powder degradation over reuse cycles. To accomplish this, we began by filling the dispenser with 20 kg of new powder and, for each print, we designed a build plate that required almost all of the powder from the dispenser. This way, most of the powder was exposed to the L-PBF process at each printing cycle. After each cycle, we mixed the remaining powder from the dispenser with the unfused powder in the collector bin (re-homogenization). After removing the build plate from the machine, we sieved all unfused powder with an 80-µm mesh, and reloaded the dispenser with the sieved powder. At each cycle, we reduced the build height by lowering the height of the print. The height was based on the quantity of powder remaining in the dispenser. This cycle was repeated eight times until there was not enough powder in the dispenser to run the next print. The applied process is summarized in Fig.1.

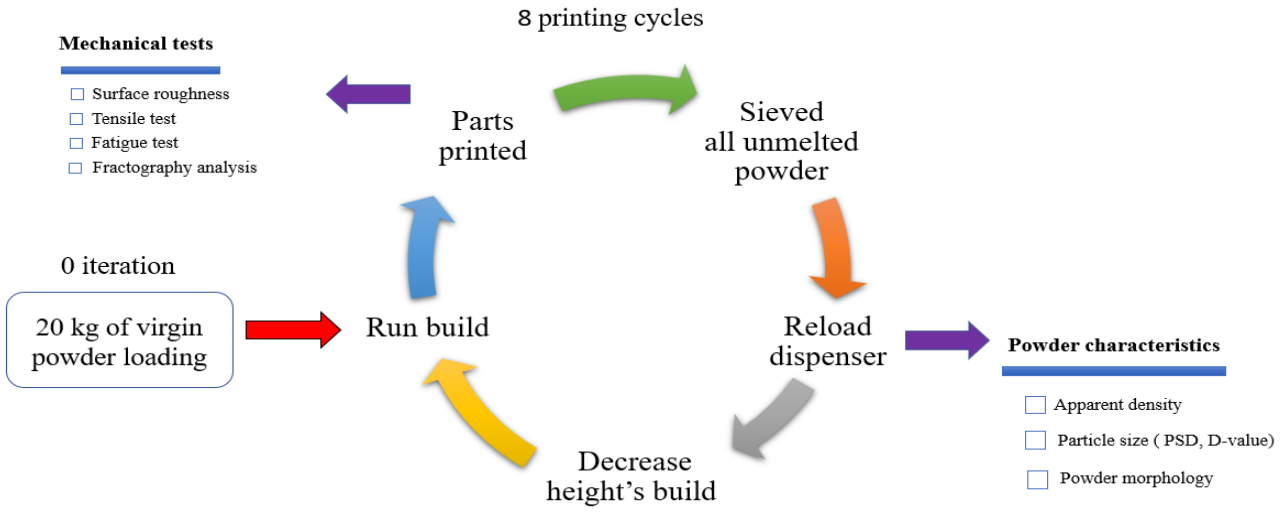

Fig.2-3 Powder recycling method

2.4 Build description and tracking parameters

Each build plate had four tensile specimens and 17 fatigue specimens printed horizontally at 0°. The geometry of the printed specimens after machining conformed to ASTM E8-a16 and ASTM E606, respectively. The final thickness of the specimen was 3 mm for both types. According to Pay *et al*. [11], the mechanical properties of parts located near the collector bin are not as good as those placed near the dispenser. Moreover, Arash Soltani-Tehrani [25] reported that the impact of powder reuse on fatigue performance was especially significant for specimens printed near the collector bin. For these two reasons, the specimens were positioned close to the collector bin. We added four sacrificial lattice structures (diameter = 40 mm and cell size = 5 mm, height = adjustable) to speed up powder contamination and, at each print, use most of the powder from the dispenser bin (see Fig.2 and Table 3).

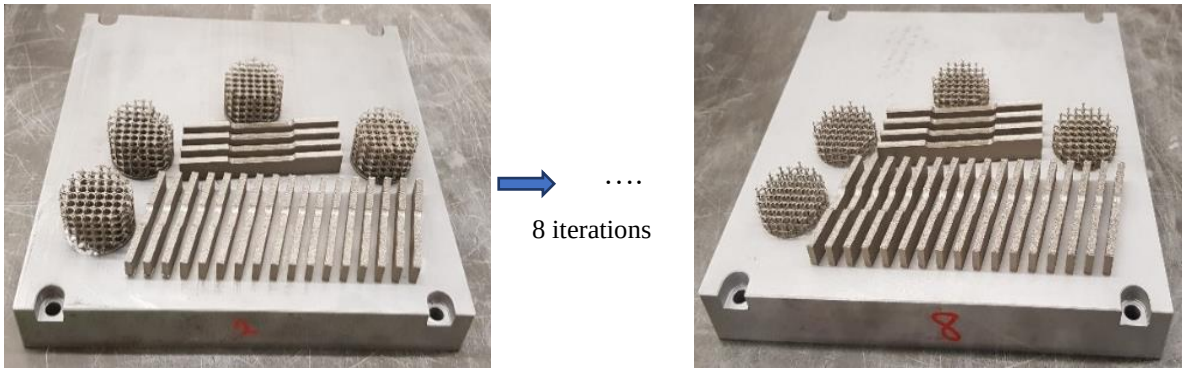

Fig.2-4 Builds description

Three important factors were monitored to accurately describe the eight-cycle printing process and to gain a better understanding of the effect of powder recycling:

1. Repetition factor: N is the number of cycles.
2. Time factors: T_{las} (h) is the laser operating time, and T_{mach} (h) is the machine operating time.
3. Quantity factors:

- Q_{con} is the powder melted and wasted after each cycle.
- H_{max} is the build's maximum height.

Table 2-2 The tracking factors of 8 builds; T_{las} (h) is the laser operating time, T_{mach} (h) is the machine operating time, Q_{con} is the powder melted and wasted, H_{max} is the build's maximum height

N	T las (h)	T mach (h)	Q con (Kg)	H max (mm)
1	6.4	11.8	2	26
2	5.8	10.6	1	24
3	5.8	10.7	1	22
4	5.7	9.7	1	20
5	5.6	9.6	1	19
6	5.6	9.8	1	17
7	5.6	10.0	1	16
8	5.5	9.0	1	14.5
Total	46.0	81.1	9.0	

After eight reuse cycles, the powder was exposed to the laser for 46 hours over a total printing period of 81 hours and the total amount of powder consumed was 9 kg.

2.4.1 Summary of powder consumption

From the 20 kg of virgin powder loaded in the dispenser, 5.63 kg was melted (28.2%), 0.78 kg (3.9%) was collected on the 80 µm sieve and discarded, 155 g (0.8%) was collected for analyzing powder morphology and PSD, and approximately 2.43 kg (12.2%) of the powder was loss during cleaning and handling, leaving 11 kg (55%) of powder after eight printing cycles (Fig.3).

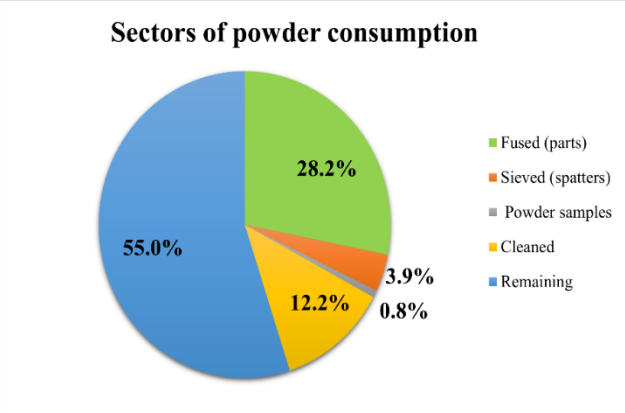

Fig.2-3 Sector of powder consumption

2.5 Post-processing

After printing, the specimens were subjected to an aging heat treatment in an ambient atmosphere. According to Kim *et al.*'s methodology [28], the maraging steel parts printed horizontally only require aging treatment at 450°C for six hours, followed by air cooling to improve their mechanical properties without using solution treatment. The aged tensile and fatigue specimens were machined in two steps using a computer numerical control (CNC) machine. The tensile and fatigue specimens geometries satisfied ASTM E8-a16 [53] and ASTM E466-15 [54] requirements, respectively, and had a final thickness of 3 mm, as shown in Fig.4 and Fig.5. All other variables of build design, printing parameters, sieving process, heat treatment and machining were carefully monitored to ensure consistency.

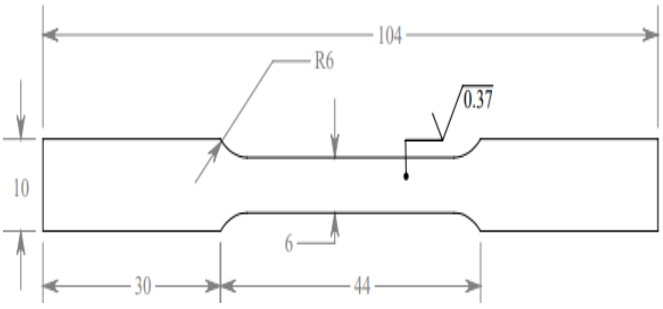

Fig.2-4 Tensile specimen. Dimensions are in mm

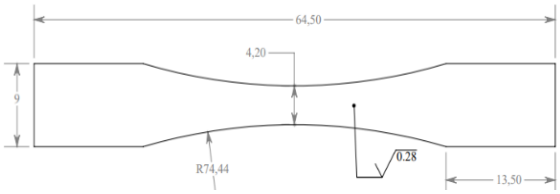

Fig.2-5 Fatigue specimen. Dimensions are in mm

2.6 Mechanical testing

The surface roughness test was conducted using a Mitutoyo FORMATRACER SV-C3100/ 4100. The profile roughness arithmetical mean deviation Ra was measured on three different fatigue as-built specimens for each printing cycle except the fourth. Five 2.5 mm-long linear measurements were performed in parallel direction with the specimen axis according to the OLDMIX standard.

The tensile tests were conducted on three tensile specimens for each cycle, with a cross-head speed of 0.5 mm/min at room temperature, according to the ASTM E8 Standard [53], using an MTS 810 servo-hydraulic machine, and employing an MTS extensometer model to measure tensile strain. Stress-controlled fatigue tests were performed using an MTS 810 machine in ambient atmosphere, applying a reversed sinusoidal load, with ratios K_t= 1 and R=0.1, adjusting the frequency to 25 Hz, and terminating at 2×10^6 cycles, according to ASTM E466-15 [54]. The mean fatigue stress amplitude S_D was determined based on the staircase method described in the French standard (Afnor) NF A03-405 [55] and Ekaputra *et al*. [56].

Lastly, the specimens' surface fractures were also analyzed using a NanoImage SNE 4500M scanning electron microscope after cleaning the specimens with ethanol.

Elemental composition of printed specimens was determined using a Bruker Esprit Compact energy dispersive X-ray spectrometer (EDS) coupled to the NanoImage scanning electron microscope. Each spectrum was acquired for 120 seconds of livetime at an accelerating voltage of 20 kV. Elements were automatically identified and quantified by the Esprit Compact software and results were normalized to 100%.

3 EXPERIMENTAL RESULTS

3.1 Powder particle size distribution

Over 8 powder reuse cycles, Dv90 increased linearly with the number of cycles ($y = 0.70x + 59.8$; $R^2 = 0.87$), resulting in an 11.4% increase of Dv90 (Fig.6). The was no significant linear regression between Dv50 or Dv10 and the number of cycles ($p > 0.05$) and the maximum difference relative to virgin powder was an increase of 6.5% and 9.1% for Dv50 and Dv10, respectively (Fig.6). Moreover, Fig.7 illustrates the evolution of powder particle size distribution (PSD). The powder had a log-normal size-distribution

with a median (Dv50) of 33.7-36.0 µm. A very small proportion of very fine particles <9 µm (0.7-0.9% of total volume) was present in all samples. A small proportion of large particles in the diameter range 200-1000 µm (1.4-3.0% of total volume) were likely aggregates since particles in this size range were not observed using the electron microscope. The PSD shifted slightly toward larger particles after eight reuse cycles (Fig.7). The larger proportion of coarser particles after powder re-use could be attributed to the formation of elongated particles, satellites, aggregate particles, and spatters, which are produced by the lattices' cylinder and are small enough to pass the 80 µm sieve. The apparent density remained stable, at 4.64 ± 0.03 g/ml over eight reuse cycles.

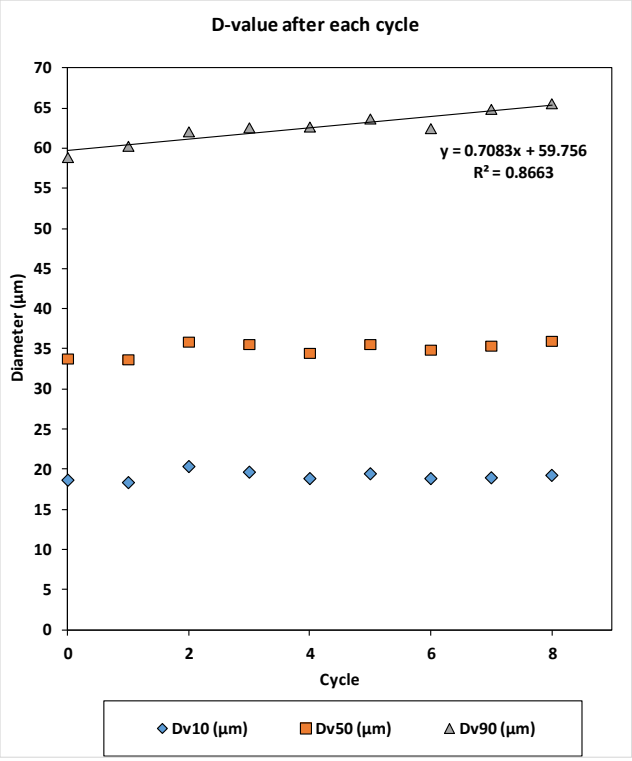

Fig.2-6 Evolution of the Dv-values over 8 printing cycles. Only Dv90 increased linearly with the number of cycles ($p < 0.001$)

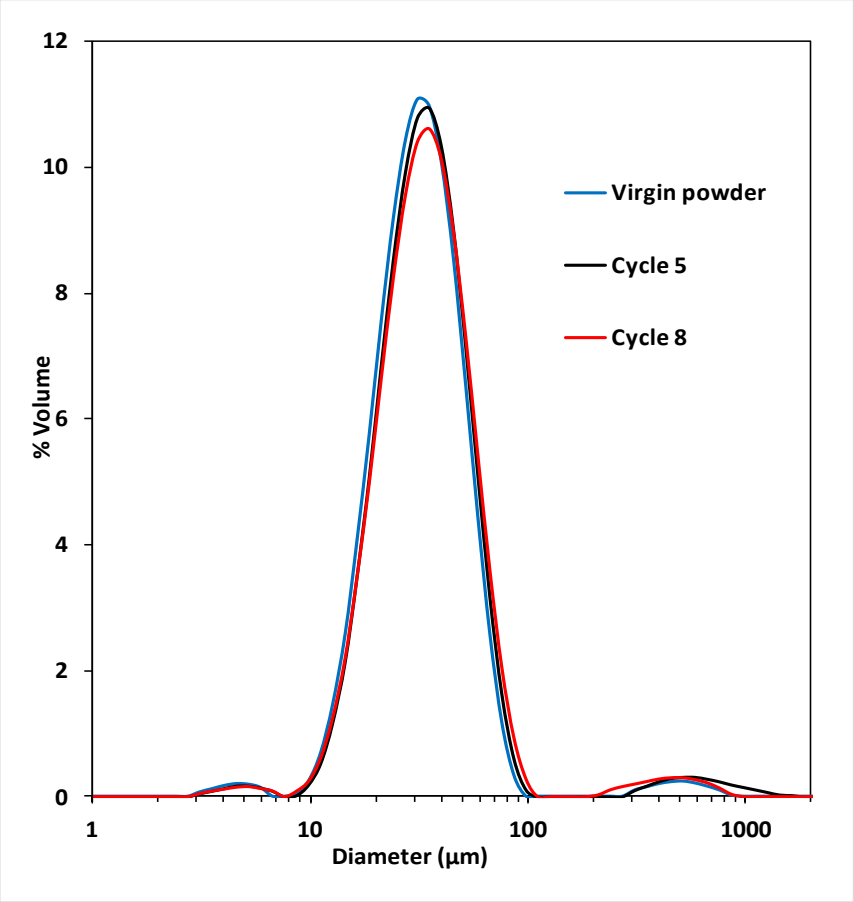

Fig.2-7 Particle size distribution of the virgin powder and of powder after 5 and 8 re-use cycles

3.2 Powder morphology

The morphology of virgin powder is globally spherical with the presence of some satellites and aggregate particles formed during the powder production process (Fig.8A) [27, 28]. The powder recycled five times (Fig.8B) and eight times (Fig.8C) exhibits shape degradation caused by the presence of aggregates, deformed particles, “clip-clap”, elongated particles, broken particles and shattered particles.

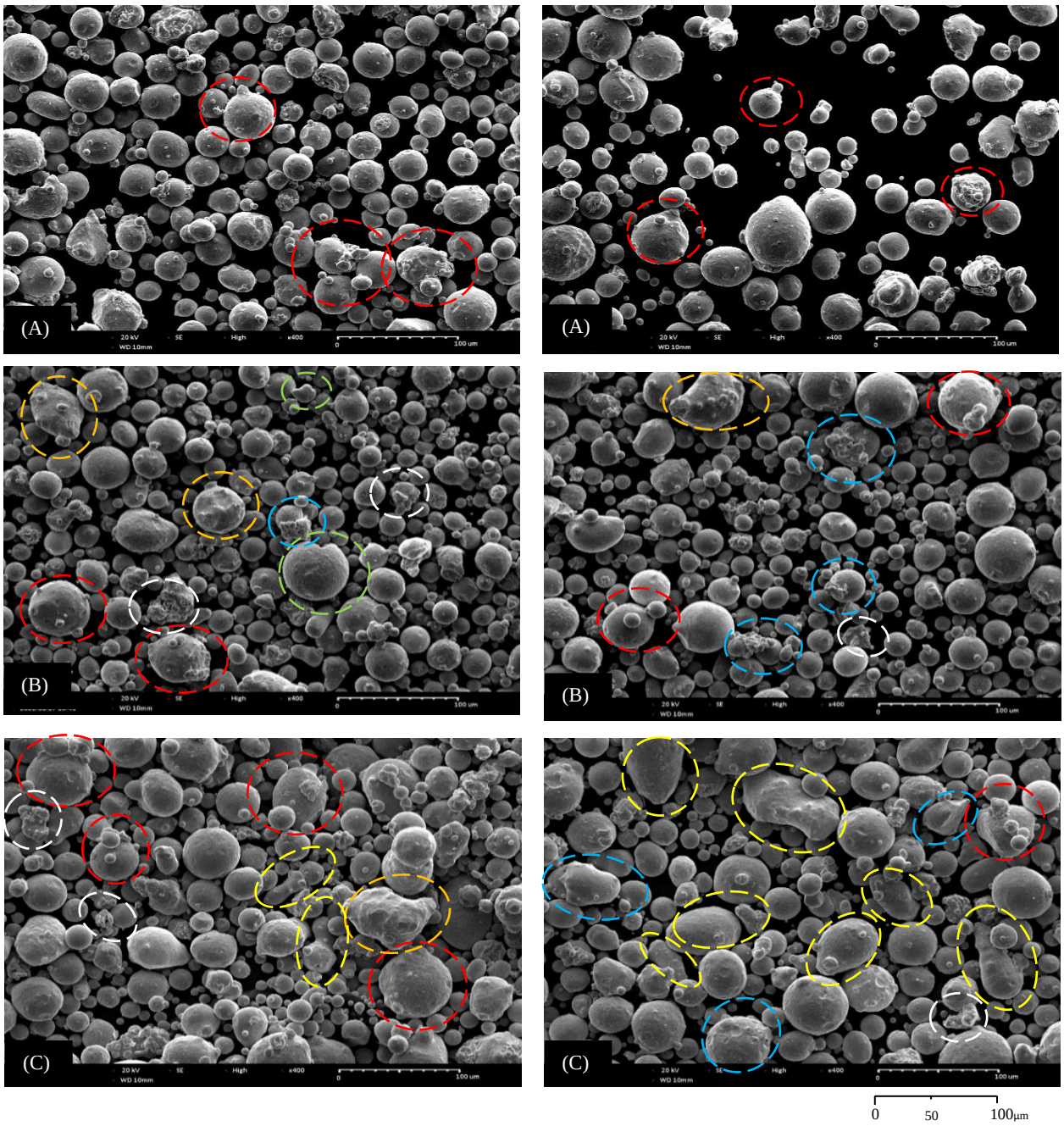

Fig.2-8 Morphologies of powder as observed using a scanning electron microscope. (A) virgin powder; (B) recycled 5 times; and (C) recycled 8 times. Color circles indicate deformed particles (orange circles), “clip-clap” (blue circles), elongated particles (yellow circles), broken particles (green circles) and shattered particles (white circles). Scale bar indicate 100 μm

3.3 Mechanical characteristics

3.3.1 Surface roughness result

Fig.9 presents the evolution of the surface roughness of as-built fatigue specimens over reuse cycles. The arithmetic mean surface roughness Ra stayed relatively constant 8.23 ± 0.43 µm. This indicates that surface roughness was not significantly impacted by reuse cycles.

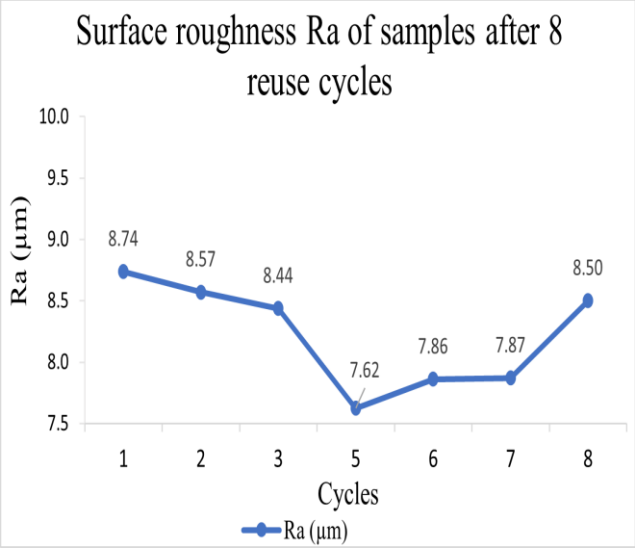

Fig.2-9 Surface roughness Ra of samples after 8

3.3.2 Tensile result

Fig.10 shows the results of the 3 measurement tensile properties for each specimen over eight reuse cycles. Ultimate tensile strength (UTS) decreased by 72 MPa (3.6%), from 1985 MPa to 1913 MPa, over eight print cycles, yield strength at 0.2% strain (0.2%YS) decreased by 58 MPa (3%), the Young module dropped by 4.5 GPa (2.4 %) and elongation at break remained stable with a low average value of 1.5% ± 0.1%.

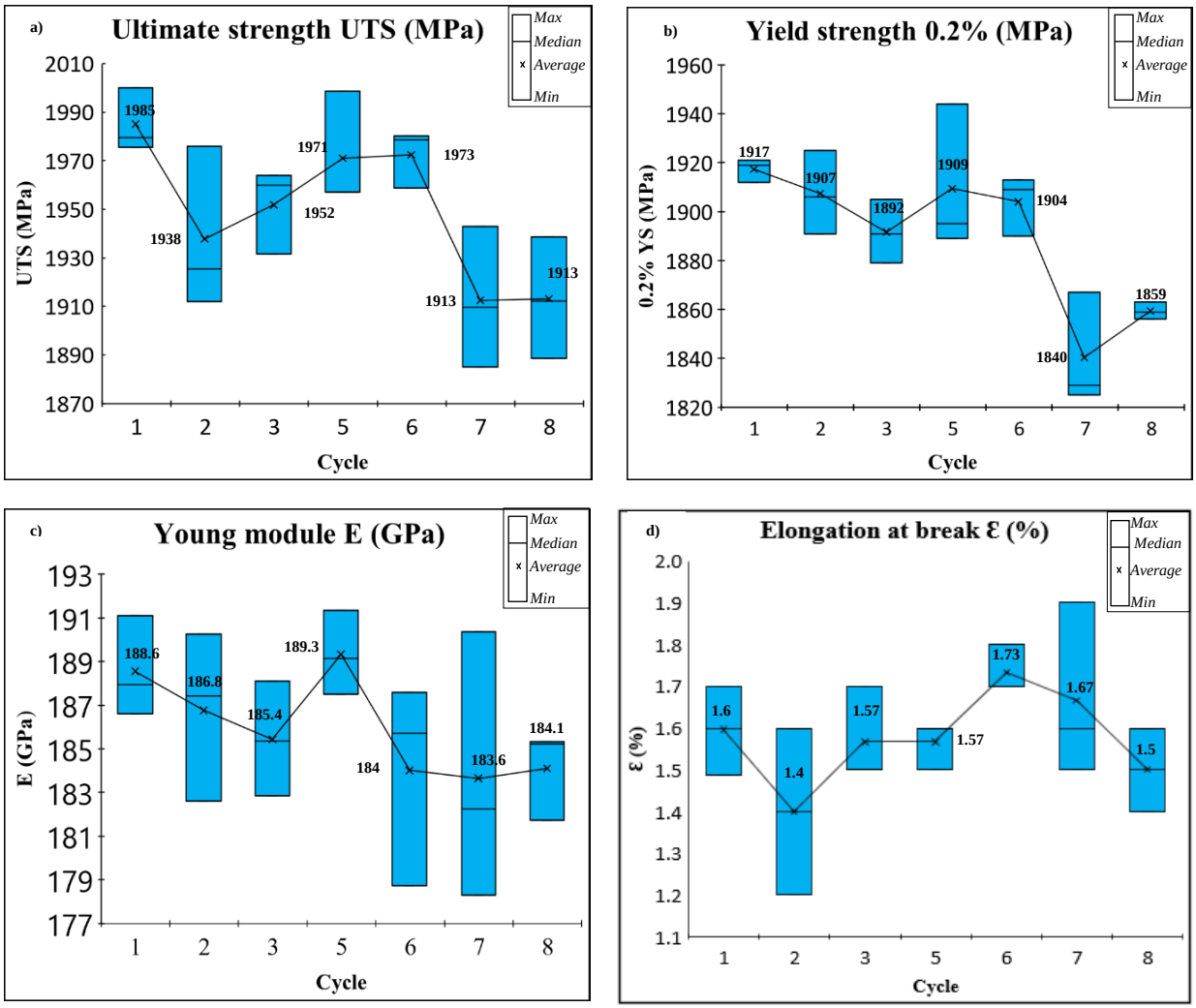

Fig.2-10 Tensile properties versus reuse times: **a)** ultimate tensile strength, **b)** yield strength, **c)** the young module and **d)** elongation at break

3.3.3 Fatigue Results

Fig.11 represents the evolution of the stress amplitude Sa applied to specimens printed in cycles 1 and 8 according to the staircase method. Five specimens for cycle 1 and seven specimens for cycle 8 reached 2 x 10^6 cycles (indicated by O). The number of failed specimens (indicated by X) is four for cycle 1 (44% failure) and seven for cycle 8 (50% failure). The parameters of the Dixon and Mood [55] approach are summarized in tables 3 and 4.

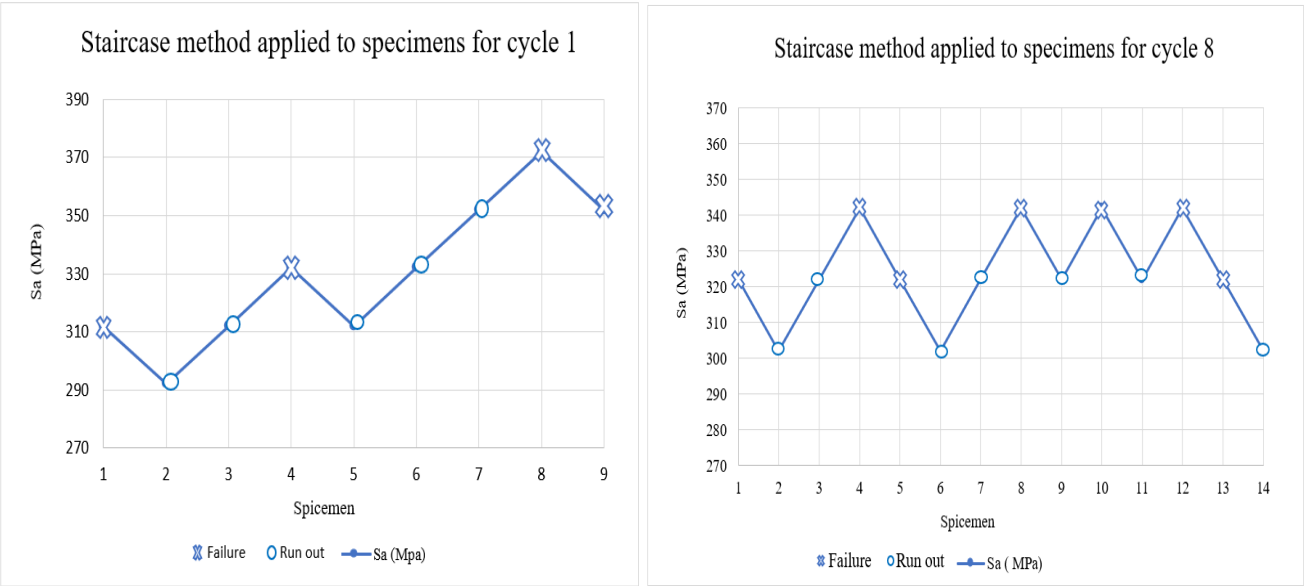

Fig.2-11 Stress amplitude (Sa) measured using the staircase test for specimens printed in cycle 1 and cycle 8

Even though the number of specimens was increased to 14 for cycle 8, the estimate of the stress standard deviation was still invalidated. According to the French standard (Afnor) NF A03-405 [55], the F_{BA} was less than 0.3 ($F_{BA} = \frac{MB-A^2}{M^2} < 0.3$). For analyzing the results of the 14 specimens in cycle 8, we used the simplified equation recommended by Ekaputra [56] and Snyder [57] to estimate standard deviation. According to the simplified equation, the standard deviation is equal to 0.53×ΔS when $F_{BA} < 0.3$, where ΔS is the step size. The fatigue test results are summarized in Table 5. The mean stress amplitude for cycle 1 is S_D = 332 (MPa), while for cycle 8 the stress is S_D = 323 (MPa). We noted that the mean stress amplitude was reduced by 2.7% from 332 to 323 (MPa), while the standard deviation decreased from 41 to 10.6 MPa after recycling the powder eight times.

Table 2-3 Parameters of i and Mi using the Dixon and Mood method for cycle 1

Stress Sa (MPa)	i	M (Mi)	A (i×Mi)	B (i×i×Mi)
372	4	1	4	16
352	3	1	3	9
332	2	1	2	4
312	1	1	1	1
292	0	0	0	0
Total	_	4	10	30

Table 2-4 Parameters of i and Mi by Dixon and Mood method for cycle 8

Stress Sa (MPa)	i	M (Mi)	A (i×Mi)	B (i×i×Mi)
342	2	4	8	16
322	1	3	3	3
302	0	0	0	0
Total	_	7	11	19

Table 2-5 Results of the staircase method

	Cycle 1	Cycle 8
S_D (MPa)	332	323
s (MPa)	41	10.6
F_{BA}	1.25	0.24

3.3.4 Fractography and EDS Analysis

SEM microscopy was employed to determine crack initiation sites for specimens of cycle 1 and 8. When applying the staircase method for specimens issued from virgin powder (cycle 1), we applied the same load 312 MPa for three specimens (1, 3 and 5) and noted that specimen 1 failed while specimens 3 and 5 survived 2 million cycles. As a result, we investigated the surface fracture of the first specimen. As seen in Fig.12a), the final breaking surface seems to be brittle and localized near the specimen's edge (indicated with the red polygon). The crack origin appears to be a lack of fusion (LOF) defect which is localized in the center in Fig.12 b). Fig.13 a) also demonstrates the surface fracture of the eighth specimen printed in cycle 1, which failed under the maximum load 372 MPa. Fig.13 b) presents lack of fusion defects and cavities. The fracture surfaces seem to be clean and contain few LOF defects (Fig.12 and Fig.13).

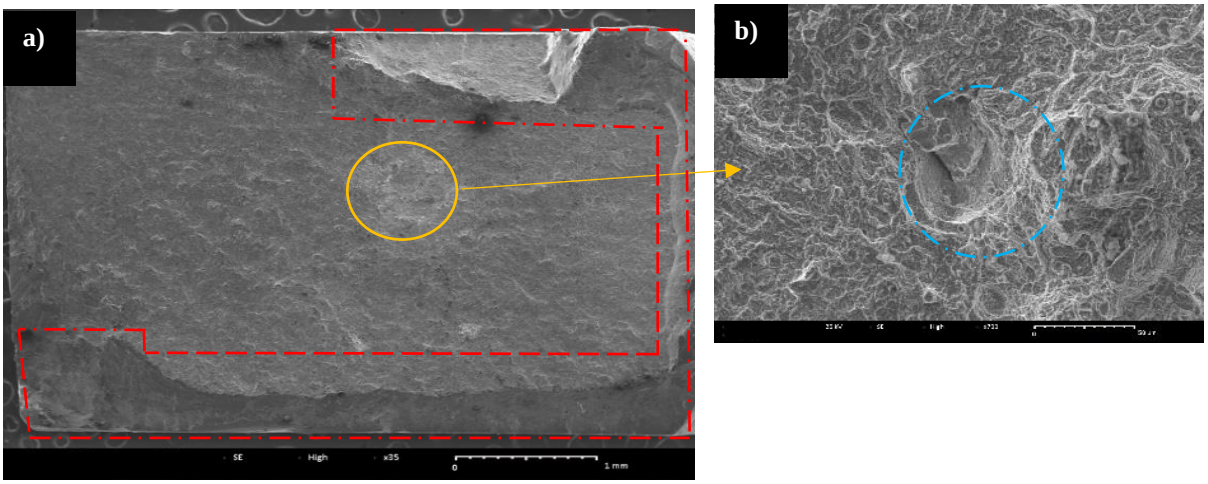

Fig.2-12 SEM images of the fracture surface of the first specimen printed in cycle 1 (S_a= 312 MPa , N= 415074); a) overview of the fracture surface at ×35, b) lack of fusion defect (LOF) at ×700

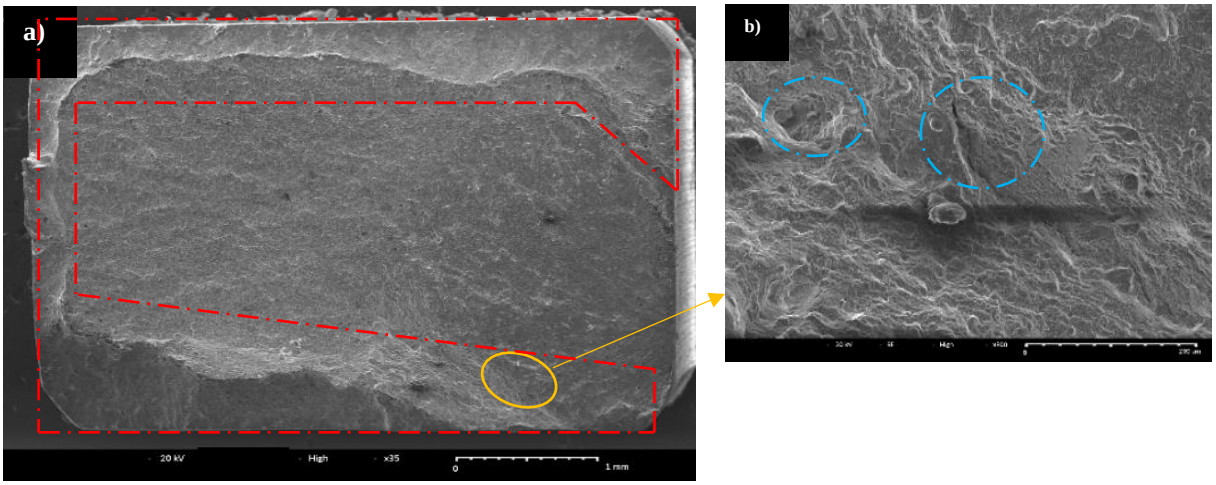

Fig.2-13 SEM images of the surface fracture of the 8th specimen printed in cycle 11 (S_a= 372 MPa , N= 297024); a) overview of the fracture surface at ×36, b) lack of fusion defect (LOF) at ×300

Using the staircase method for specimens produced from cycle 8, we applied the same load 322 MPa to two specimens: the first specimen failed early at 63,081 cycles, while the second specimen survived 2 million cycles. Subsequently, we chose to investigate the probable defect of the failed part. Fig.14 a) shows an overview of the fracture surface at ×36 magnification factor. The final breaking surface of the specimens is bounded by the red dotted polygon. The fracture surface of this specimen shows a substantial presence of defects that could lead to crack initiation and failure: Fig.14 b) and Fig.14 c) represent,

respectively, a partially melted particle defect (indicated by a green circle), and inclusion defect (indicated by an orange circle). Fig.14 d) illustrates a partially melted particles defect and LOF defect (indicated by a blue circle). Fig.14 e) reveals the presence of an inclusion defect which has a spherical form and is highly agglomerated (indicated by an orange circle), whereas Fig.14 f) illustrates this inclusion in the backscattered electrons mode (BSE). The melted metal appears grey, while the inclusion is black (indicated by an orange circle) suggests that this inclusion could be rich in carbon.

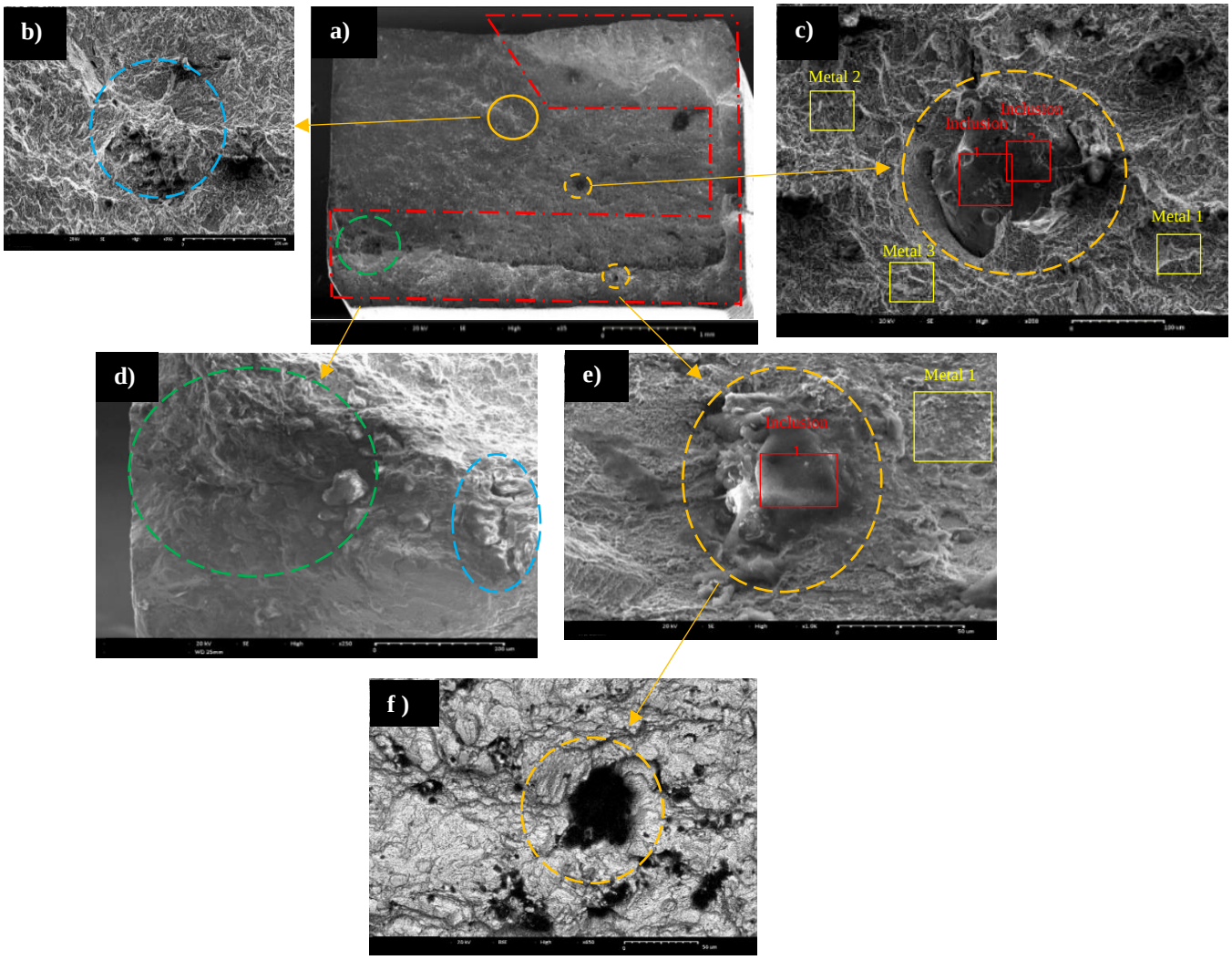

Fig.2-14 SEM images of the surface fracture of the first specimen printed in cycle 8 (S_a= 322 MPa , N= 63081) , a) overview of the fracture surface at ×36, b) LOF defect at ×300, c) LOF defect and inclusion at ×300, d) partially melted particles and LOF defect at ×200, e) inclusion defect (spatter) at ×1000, f) BSE mode of image e) at × 650. Yellow and red boxes indicate the position of the EDS measurements

Table 6 and 7 present the results of the EDS analysis applied to this specimen. The chemical composition of inclusions shown in Fig.14 c) and Fig.14 (e, f) are presented in table 6 and 7 respectively. As can be noted in table 6, the composition of the inclusion is quite similar to those measured in the metal regions, which confirms that this inclusion is a metal particle. Moreover, it was reported that spatters had similar chemical composition to the virgin powder composition [50]. Consequently, this metal inclusion could be a spatter that was previously present in the recycled powder or produced during the printing process.

However, the inclusion displayed in Fig.14 (e, f) shows a relevant presence of 76.4% of carbon and a small percentage of iron Fe 10.1 %, while the metal disposed around contain less carbon C 24.5 % and a substantial percentage of iron Fe 40.3 %. Thus, we can conclude that this inclusion is a carbon inclusion.

Table 2-6 Elemental composition of the inclusion presented in Fig.14 c) and surrounding metal (in mass percent)

Spectrum	C	O	Al	Si	Ti	Fe	Co	Ni
Inclusion spectra 1	15.3	10.0	7.2	2.6	0.9	50.1	8.3	5.6
Inclusion spectra 2	13.2	2.9	0.4	0.2	0.8	59.2	8.5	14.8
Metal spectra 1	11.6	2.8	1.4	0.2	0.6	61.0	9.5	12.9
Metal spectra 2	11.6	4.2	2.0	0.1	4.9	55.2	8.1	13.9
Metal spectra 3	10.9	3.1	0.3	0.1	0.7	60.1	9.8	15.0

Table 2-7 Elemental composition of the inclusion presented in Fig.14 (e, f) and surrounding metal (in mass percent)

Spectrum	C	O	Al	Si	Ti	Fe	Co	Ni
Inclusion spectra 1	76.4	9.6	0.5	0.2	0.1	10.1	1.2	1.9
Metal spectra 1	24.5	15.0	3.9	0.4	0.6	40.3	5.6	9.8

Moreover, the fatigue specimens 4, 8, 10 and 12 printed in the eighth reuse cycle failed very early under the maximum stress load 342 MPa. The broken surface of specimen 10 was examined. As can be seen in Fig.15, more internal defects, such as lack of fusion, partially melted particles and gas pores (indicated by a purple circle) are apparent on the specimen's surface. This surface fracture has a high prevalence of fusion defects, generating many gaps and pores, and could be the main reason for fracture initiation and failure.

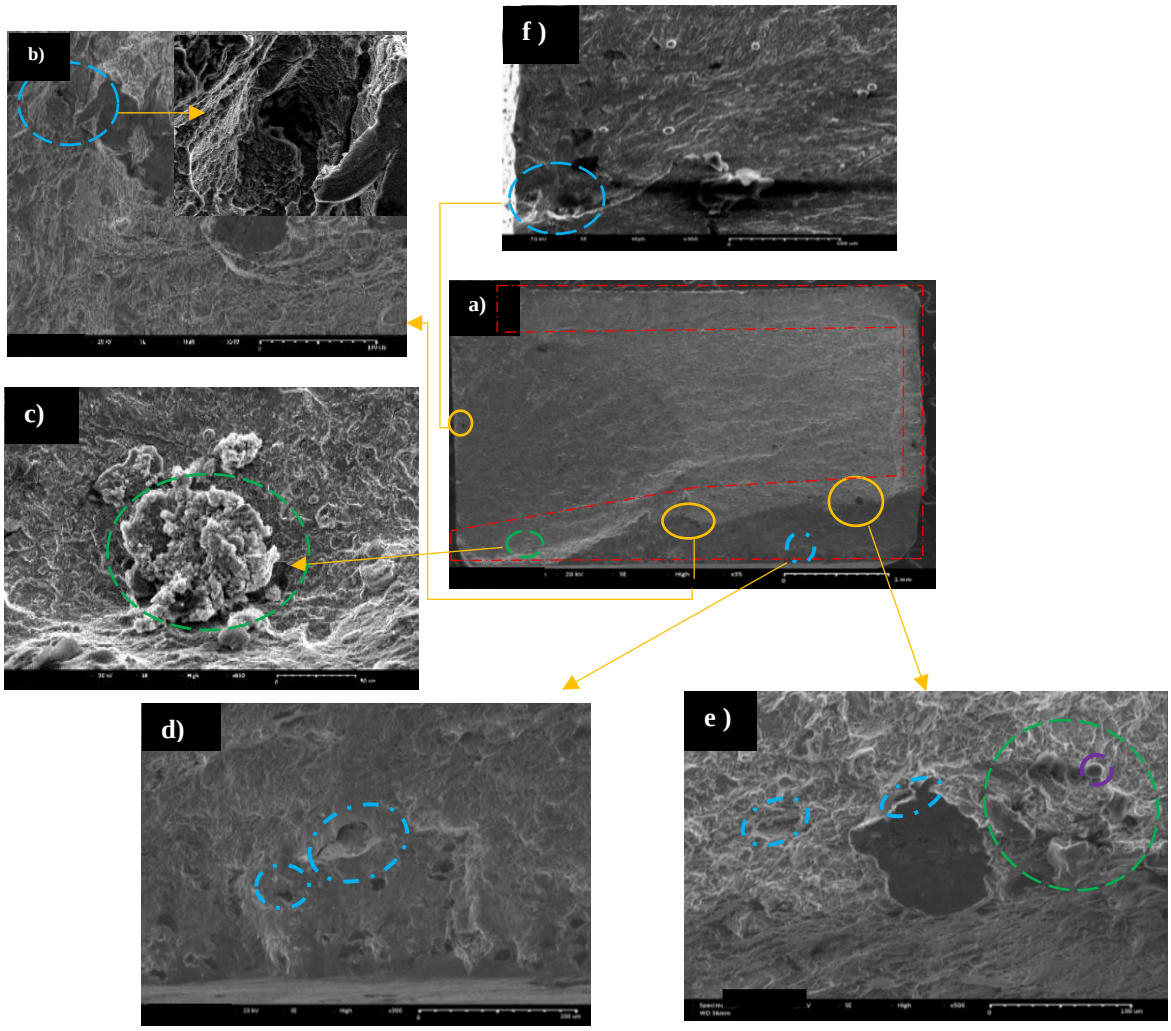

Fig.2-15 SEM images of the first surface fracture of the 10th specimen printed in cycle 8 (S_a=342 MPa , N= 152109), a) overview of the fracture surface at ×35, b) LOF defect at ×500, c) partially melted particle defect at ×650, d) LOF defect at ×400 , e) LOF defect, partially melted particles and gas pores at ×500, f) lack of fusion defects (crack origin) at ×300

4 DISCUSSION

The powder PSD was only slightly affected by powder recycling; the most significant effect was a 11% increase in Dv90 after 8 reuse cycles compared to the virgin powder. Recent studies have shown that particle size distribution PSD became narrower after reuse cycles, indicating a decrease in the proportion of fine particles involved in the melting process, followed by a drop in the quantity of larger particles, which were reduced progressively by the sieve device after reuse [9, 14, 16, 17, 24, 36, 42, 43]. Soundarapandiyan [22] and Richard and O'Leary [7] confirmed our findings by reporting the same behavior of the Ti-6Al-4V powder PSD, which shifted rightward after five reuse cycles. Furthermore, Sutton *et al*. [17] found comparable results using AISI 304L stainless steel powder, demonstrating an increase in particle size after five printing cycles. V. Contaldi [14] discovered that the PSD of martensitic PH1 powder shifted to the right due to agglomeration as the smallest particles passed through the sieve device, resulting in an increase in the quantity of larger particles after nine times reuse. These findings align with our observations. However, the PSD of austenitic GP1 powder was narrowed and moved to the left, showing a decrease of fine and larger particle proportions. They concluded that the differences in PH1 and GP1 PSDs could be attributed to noise, handling, and manual sieving, all of which could induce uncertainty.

Powder particles shape was also drastically affected after eight reuse cycles with an increase in particle roughness and the presence of a large proportion of partly fused powder. These changes in recycled powder morphology are due to the presence of spatters (Szost *et al*. [19]; Renishaw 2016 [34]) and to laser heat exposure that sinters the particles and induces their mechanical deformation (Shanbhag [37], Renishaw 2016 [34] and Popov [33]). Even if most spatters are eliminated by sieving at 80 µm, smaller spatters pass through the sieve and influence the shape of recycled powder (Rock *et al*. [23]; Sutton *et al*. [31, 42]).

Normally, the powder size should be reduced when the powder passes multiples times through the sieve device, however in this study the powder size increased mildly. A possible reason could be due to its shape alteration caused by laser heat and the formation of aggregates that could pass through the sieve device.

Although the alteration of powder size and morphology, the powder apparent density remained constant 4.64 ± 0.03 g/ml after eight printing cycles, as was also reported by Contaldi [41]. However, Del Re *et al*. [16] noted a slight increase in the tap density of aluminum AlSi10Mg powder over eight reuse cycles.

Regarding the surface roughness of as-built parts, Ra showed a mild variation around 7.62 and 8.74 µm over eight printing cycles. According to Del Re *et al.* [16], the surface roughness of AlSi10Mg parts

remained constant over eight cycles. However, V. Seyda [43] discovered an important increase of 33.7% in the horizontal 10-point mean roughness Rz for titanium parts produced 12 times. The surface became rougher due to the increased proportion of larger particles after the reuse process.

As previously demonstrated, the tensile properties of maraging steel parts reduced slightly by 3% after 8 reuse cycles. Similar result was reported by Del Re *et al*. [16], they concluded that the yield and tensile strength of AlSi10Mg components dropped by 10 MPa, while elongation at break was around 18% after eight reuse cycles. This slight decrease was attributed to the powder storage and recycling methods (collective aging). Furthermore, Sun *et al*. [14] concluded that parts printed from maraging steel powder reused 113 times had identical static properties compared with ones produced from virgin powder. However, Seyda *et al*. [43] reported a slight amelioration of tensile properties after recycling titanium powder 12 times due to the increase in the percentage of oxygen oxide within printed parts. Moreover, Popov *et al*. [33] found that both UTS and YS increased slightly after reusing titanium powder 69 times, while elongation was substantially reduced because of residual surface oxidation and surface defects of the recycled powder particles.

Many studies have confirmed our findings and reported the impact of powder reuse on the fatigue performance of printed parts. Del Re *et al*. [16] discovered a decrease of 10.3% on fatigue strength after reusing AlSi10Mg powder eight times, while Popov *et al*. [13] found that Ti-6Al-4V part fatigue endurance was dramatically impacted after reuse due to porosity, partly melted particles, and lack of fusion (LOF) defects. However, Carrion *et al*. [6] and Arash Soltani-Tehrani [25] discovered that powder recycling enhanced respectively the fatigue properties of Ti-6Al-4V and 17-4 PH stainless steel machined components in the high cycle regime, owing to enhanced powder flowability over powder reusing, which results in a more uniform powder bed layer and potentially fewer pores within parts. The unmachined specimens were not impacted by the reuse cycles. It was concluded that fatigue performance depends substantially on the surface condition of printed parts, and the effect of powder reuse is remarkable only on machined parts.

Furthermore, the fractography and EDS analyses revealed that parts printed from new powder did not show a significant presence of internal imperfections. Significant pores, carbon inclusion and LOF defects were detected on the surface fracture of specimens printed from reused powder, which could be the result of powder degradation. The spatters generated by the melting process are deposited in the powder bed, which will undoubtedly affects not only the powder quality but also creates pores and inclusions within the melted part [18, 38]. Additionally, Pal *et al*. [11] reported that powder size and morphology affect the

formation of melt pools during the melting process by creating more spatters. The proportion of porosity inside parts increased, which reduced the parts' mechanical properties. Moreover, Carrion *et al*. [24] reported that reusing powder led to the creation of smaller pores inside titanium parts. However, Soltani-Tehrani [25] reported that both 17-4 PH stainless steel parts printed from new and reused powder exhibited internal defects, such as LOF defects and gas pores, but powder reuse significantly decreased pore size, which ameliorated part fatigue performance. Furthermore, Popov *et al*. [33] reported that (HIP) heat treatment is an effective way to reduce gas pores, however, it does not eliminate LOF defects inside parts made from reused powder. Moreover, both Gatto [50] and Sun *et al*. [14] discovered that the fracture surfaces of maraging steel parts, produced from cross-contaminated powder and from recycled powder, respectively, contained a substantial amount of Ti-Al oxide inclusions, cavities and pores. The effect of this inclusion was more relevant with respect to part fatigue performance, while tensile mechanical properties seem to be less sensitive to these defects thanks to material ductility.

After powder reuse, mean fatigue strength decreased by 2.7%, from 332 to 323 (MPa), and the stress standard deviation became narrower (± 10.6 MPa). This would suggest that all parts printed in cycle 8 exhibit similar fatigue behavior, while parts made from fresh powder had a wide standard deviation (± 41 MPa), possibly caused by the more random presence of defects. The fractography and EDS analysis show that fusion defects are hugely present in parts made from eight times recycled powder, which could explain why the stress standard deviation of these components is narrower. Nevertheless, it is important to mention that fatigue behavior is intrinsically uncertain, since it depends on the surface condition, the existence of imperfections within the part, and the part's physiological properties, especially for AM components [16].

Indeed, as investigated above, parts produced from reused powder exhibit a relevant presence of pores, LOF and carbon inclusion defects, which could also explain this slight decrease in the parts' mechanical performance. However, this small reduction of approximately 3% in tensile properties and fatigue performance could be ascribed to the re-homogenization of reused powder (mixing reused powder with dispenser's powder after each cycle): the reused powder that was spread over the build plate and over the collector bin was re-homogenized with approximately 3 kg of powder remaining in the dispenser after each print, which made it possible to slow down the degradation effect on its properties over reuse time, although there was a slight alteration of powder size and morphology caused by the L-PBF process and lattice parts.

5 CONCLUSION

Maraging steel powder was reused eight times in the L-PBF process in this study using a recycling approach which maximized powder degradation. The effect of powder reuse on particle size distribution, particle morphology and apparent density, as well as on the evolution of the surface roughness and mechanical properties of manufactured parts, were investigated in order to bridge the gap in knowledge regarding the impact of maraging steel powder reuse, particularly on part fatigue performance. The following conclusions can be made from the experimental results and observations:

- Particle size distribution (PSD) shifted slightly toward larger particles over eight printing cycles, with D90 increasing linearly by 11.4%. The electron microscope images confirmed the degradation of particle shapes over reuse cycles by the presence of aggregates, deformed and elongated particles, "clip-clap" particles, broken and shattered particles, which could pass through the 80 µm sieve and contribute to an increase in the proportion of large particles. The slight increase in particle size had no effect on the apparent density of sieved powder which remained stable at 4.64 ± 0.03 g/ml through all eight cycles. The arithmetic surface roughness Ra of as-built parts showed a slight variation of average 8.23 ± 0.43 µm over eight printing cycles, indicating that the impact of powder reuse was negligible on the surface roughness of maraging steel parts.

- It was discovered that consuming approximately 9 kg (45%) from 20 kg of maraging steel virgin powder, which was loaded initially in the feeder and passed through eight collective aging cycles, taking a total of 81 hours of printing time and 46 hours of laser operating time, slightly affected the tensile properties of specimens: ultimate tensile strength (UTS) decreased by 3.6%, from 1985 MPa to 1913 MPa, yield strength (0.2% YS) dropped by 3%, from 1917 MPa to 1859 MPa, while the Young module was reduced by 2.6%, from 189 GPa to 184 GPa, and elongation at break stayed stable around 1.58% ±0.1%.

- Generally, fatigue behavior remained constant despite a minor decrease over reuse cycles. The mean stress amplitude decreased by 2.7%, from 332 to 323 (MPa), while the standard deviation decreased from 41 to 10.6 MPa after recycling the powder eight times. Indicating that the results are more grouped and therefore less dispersed. It is assumed that this effect is caused by a larger quantity of fusion defects and more uniformly distributed in the parts produced from reused powder. Finally, the fractographic study confirms this hypothesis .

- Fractography and EDS analysis proved that the fracture surface of specimens printed from virgin powder contained fewer internal defects compared with specimens printed from recycled powder, which had a relevant presence of pores, partially melted particle defects, gas pores, lack of fusion (LOF) defects and carbon inclusion defects. These defects were most likely formed as a result of the alterations in the powder's properties and the effect of the melting process during the reuse cycles.

CONCLUSION GÉNÉRALE

En premier lieu, l'altération de la poudre acier maraging causée par le processus d'impression 3D et par le recyclage de la poudre a été étudié. Précisément, l'effet du processus de fusion de poudre, l'emplacement des pièces, la distance entre les pièces imprimées et les caractéristiques géométriques des pièces. Ainsi, le PSD et la morphologie de la poudre recyclée a été évalués. Les résultats montrent que la taille des particules de poudre n'est pas uniformément distribuée sur le lit de poudre. Les particules sont plus grosses proche du collecteur et plus petite près du distributeur de poudre. La taille de la poudre tamisée diminue légèrement durant un seul cycle d'impression. Toutefois, le système de filtration des gaz qui transporte les éclaboussures et les fumées n'a pas d'effet notable sur le PSD de la poudre. Le PSD du lit de poudre se déplace vers les particules plus grosses avec une baisse considérable du pourcentage de particules fines lorsque la distance entre les pièces imprimées diminue. Les structures de treillis (lattices) ont un impact remarquable sur le PSD du lit de poudre. Ils produisent une quantité énorme d'éclaboussures, d'agrégats, de particules allongées et déformées. Finalement, après 12 cycles d'impression, les particules de la poudre sont devenues plus grosses et leur morphologie a été significativement altérée.

Dans le deuxième article, les travaux ont porté sur l'effet du recyclage de la poudre sur les performances mécaniques des pièces imprimées en acier maraging. La poudre a été recyclée 8 fois sans ajout de poudre neuve et en diminuant la hauteur du volume d'impression après chaque cycle. Les impressions contiennent des éprouvettes et des cylindres en treillis. Encore une fois, les résultats montrent que la taille de la poudre augmente après 8 cycles et que la morphologie des particules est altérée par la présence d'agrégats, de particules allongées et déformées. Aucun changement de la densité apparente de la poudre n'a toutefois été mesurée. Aucun impact mesurable du recyclage sur la rugosité de surface des pièces telles que imprimées n'a été remarqué. Malgré une légère diminution des propriétés

mécaniques approximativement 3% au cours des cycles de réutilisation, les performances en traction et en fatigue sont restées globalement stables. L'écart type de la limite d'endurance des éprouvettes provenant de la poudre recyclée est étroit, indiquant que les résultats sont plus regroupés et donc moins dispersés. On fait l'hypothèse que cet effet est causé par une quantité de défauts plus importante et répartie de façon plus uniforme dans les pièces. Finalement, l'étude fractographique et l'analyse EDS viennent confirmer cette hypothèse en démontrant que les faciès de rupture en fatigue des composants fabriqués à partir de la poudre réutilisée 8 fois présentent plus de porosités, de manques de fusion et des défauts d'inclusion par rapport aux pièces fabriquées à partir de poudre neuve.

En guise de conclusion, on peut affirmer que le processus de fusion de la poudre (L-PBF) appliqué à des pièces de différentes géométries (simple et structure en treillis) affectent de façon mesurable les caractéristiques granulométriques et morphologiques du lit de poudre. Les résultats montrent aussi que le recyclage affecte très peu les propriétés mécaniques moyennes des pièces imprimées. Toutefois, les pièces imprimées avec la poudre recyclée contiennent plus des défauts d'inclusion et de manque de fusion, ce qui pourrait expliquer que l'écart type de la limite d'endurance des éprouvettes fabriqués avec la poudre recyclée est plus petit que celui des pièces fabriquées avec la poudre neuve.

En terminant, rappelons que les effets du recyclage de la poudre rapportés dans la littérature [9, 15, 16, 21, 24, 25, 33] sont fonction de la méthode de recyclage adoptée, du nombre de cycles de recyclage, des paramètres du laser, du matériau et de la densité d'impression. Il serait intéressant de répéter les travaux présentés dans ce document sur un autre matériau que l'acier maraging pour déterminer si d'autres matériaux subiraient les mêmes changements que celui présenté dans cette étude. Comme le sujet du recyclage de la poudre d'acier maraging est moins abordé dans les travaux de recherche, il serait intéressant d'étudier l'effet du recyclage de cette poudre dans des conditions extrêmes en augmentant le nombre de recyclage à 30 fois ou plus, ce qui aurait pour effet d'altérer de façon plus importante les caractéristiques de la poudre. Concernant le comportement en fatigue des pièces imprimées au 8ème cycle, il a été remarqué que l'écart-type des contraintes alternées

était plus étroit que celui des éprouvettes imprimées au 1er cycle. On pourrait penser que les éprouvettes provenant de la poudre recyclée seraient toutes identiques en ce qui concerne la présence de défauts d'inclusion, ce qui réduirait l'écart-type. Cette hypothèse a été confirmée par notre analyse fractographique. Cependant, il pourrait être intéressant de clarifier davantage ce résultat . Pour ce faire, il est recommandé d'augmenter le nombre d'éprouvettes testées par la méthode de l'escalier à 15, tel que le recommande l'AFNOR [55].

RÉFÉRENCES BIBLIOGRAPHIQUES

[1] O. Diegel, A. Nordin, and D. Motte, *A practical guide to design for additive manufacturing*. Springer, 2019.

[2] D. Kim *et al.*, "Effect of Heat Treatment Condition on Microstructural and Mechanical Anisotropies of Selective Laser Melted Maraging 18Ni-300 Steel," *Metals,* vol. 10, no. 3, 2020, doi: 10.3390/met10030410.

[3] E. G.-E. O. Systems, "EOS MaragingSteel MS1 DATA SHEET," 2017. [Online]. Available: www.eos.info.

[4] J. C. Najmon, S. Raeisi, and A. Tovar, "Review of additive manufacturing technologies and applications in the aerospace industry," *Additive manufacturing for the aerospace industry,* pp. 7-31, 2019.

[5] R. Liu, Z. Wang, T. Sparks, F. Liou, and J. Newkirk, "Aerospace applications of laser additive manufacturing," in *Laser additive manufacturing*: Elsevier, 2017, pp. 351-371.

[6] J. H. Tan, W. L. E. Wong, and K. W. Dalgarno, "An overview of powder granulometry on feedstock and part performance in the selective laser melting process," *Additive Manufacturing,* vol. 18, pp. 228-255, 2017, doi: 10.1016/j.addma.2017.10.011.

[7] G. Soundarapandiyan, C. Johnston, R. H. U. Khan, B. Chen, and M. E. Fitzpatrick, "A technical review of the challenges of powder recycling in the laser powder bed fusion additive manufacturing process," *The Journal of Engineering,* vol. 2021, no. 2, pp. 97-103, 2021, doi: 10.1049/tje2.12013.

[8] D. Powell, A. E. W. Rennie, L. Geekie, and N. Burns, "Understanding powder degradation in metal additive manufacturing to allow the upcycling of recycled powders," *Journal of Cleaner Production,* vol. 268, 2020, doi: 10.1016/j.jclepro.2020.122077.

[9] F. J. Alamos *et al.*, "Effect of powder reuse on mechanical properties of Ti-6Al-4V produced through selective laser melting," *International Journal of Refractory Metals and Hard Materials,* vol. 91, 2020, doi: 10.1016/j.ijrmhm.2020.105273.

[10] M. Lutter-Günther, C. Gebbe, T. Kamps, C. Seidel, and G. Reinhart, "Powder recycling in laser beam melting: strategies, consumption modeling and influence on resource efficiency," *Production Engineering,* vol. 12, no. 3-4, pp. 377-389, 2018, doi: 10.1007/s11740-018-0790-7.

[11] S. Pal *et al.*, "The effects of locations on the build tray on the quality of specimens in powder bed additive manufacturing," *The International Journal of Advanced Manufacturing Technology,* vol. 112, no. 3-4, pp. 1159-1170, 2021, doi: 10.1007/s00170-020-06563-5.

[12] A. B. Anwar and Q.-c. Pham, "Effect Of Inert Gas Flow Velocity And Unidirectional" 2016.

[13] P. Moghimian *et al.*, "Metal powders in additive manufacturing: A review on reusability and recyclability of common titanium, nickel and aluminum alloys," *Additive Manufacturing,* vol. 43, 2021, doi: 10.1016/j.addma.2021.102017.

[14] H. Sun, X. Chu, Z. Liu, A. Gisele, and Y. Zou, "Selective Laser Melting of Maraging Steels Using Recycled Powders: A Comprehensive Microstructural and Mechanical Investigation," *Metallurgical and Materials Transactions A,* vol. 52, no. 5, pp. 1714-1722, 2021, doi: 10.1007/s11661-021-06180-1.

[15] A. T. Sutton *et al.*, "Evolution of AISI 304L stainless steel part properties due to powder recycling in laser powder-bed fusion," *Additive Manufacturing,* vol. 36, 2020, doi: 10.1016/j.addma.2020.101439.

[16] F. Del Re *et al.*, "Statistical approach for assessing the effect of powder reuse on the final quality of AlSi10Mg parts produced by laser powder bed fusion additive manufacturing," *The International Journal of Advanced Manufacturing Technology,* vol. 97, no. 5-8, pp. 2231-2240, 2018, doi: 10.1007/s00170-018-2090-y.

[17] O. A. Quintana, J. Alvarez, R. McMillan, W. Tong, and C. Tomonto, "Effects of Reusing Ti-6Al-4V Powder in a Selective Laser Melting Additive System Operated in an Industrial Setting," *Jom,* vol. 70, no. 9, pp. 1863-1869, 2018, doi: 10.1007/s11837-018-3011-0.

[18] C. S. K. Austin T. Sutton, Sreekar Karnati, Ming C. Leu, Joseph W. Newkirk, "Characterization of AISI 304L Stainless Steel Powder Recycled in the Laser Powder-Bed Fusion Process," *Additive Manufacturing,* vol. 32, p. 100981, 2020.

[19] B. Szost, X. Wang, D. Johns, S. Sharma, A. Clare, and I. Ashcroft, "Spatter and oxide formation in laser powder bed fusion of Inconel 718," *Additive manufacturing,* vol. 24, pp. 446-456, 2018.

[20] F. Yi, Q. Zhou, C. Wang, Z. Yan, and B. Liu, "Effect of powder reuse on powder characteristics and properties of Inconel 718 parts produced by selective laser melting," *Journal of Materials Research and Technology,* vol. 13, pp. 524-533, 2021, doi: 10.1016/j.jmrt.2021.04.091.

[21] G. Shanbhag and M. Vlasea, "The effect of reuse cycles on Ti-6Al-4V powder properties processed by electron beam powder bed fusion," *Manufacturing Letters,* vol. 25, pp. 60-63, 2020, doi: 10.1016/j.mfglet.2020.07.007.

[22] G. Soundarapandiyan *et al.*, "The effects of powder reuse on the mechanical response of electron beam additively manufactured Ti6Al4V parts," *Additive Manufacturing,* vol. 46, 2021, doi: 10.1016/j.addma.2021.102101.

[23] S. E. Brika, M. Letenneur, C. A. Dion, and V. Brailovski, "Influence of particle morphology and size distribution on the powder flowability and laser powder bed fusion manufacturability of Ti-6Al-4V alloy," *Additive Manufacturing,* vol. 31, p. 100929, 2020.

[24] P. E. Carrion, A. Soltani-Tehrani, N. Phan, and N. Shamsaei, "Powder Recycling Effects on the Tensile and Fatigue Behavior of Additively Manufactured Ti-6Al-4V Parts," *Jom,* vol. 71, no. 3, pp. 963-973, 2018, doi: 10.1007/s11837-018-3248-7.

[25] A. Soltani-Tehrani, J. Pegues, and N. Shamsaei, "Fatigue behavior of additively manufactured 17-4 PH stainless steel: The effects of part location and powder re-use," *Additive Manufacturing*, vol. 36, p. 101398, 2020.
[26] Y. Zhu *et al.*, "3D printing biomimetic materials and structures for biomedical applications," *Bio-Design and Manufacturing*, vol. 4, no. 2, pp. 405-428, 2021.
[27] J. Dawes, R. Bowerman, and R. Trepleton, "Introduction to the Additive Manufacturing Powder Metallurgy Supply Chain," *Johnson Matthey Technology Review*, vol. 59, no. 3, pp. 243-256, 2015, doi: 10.1595/205651315x688686.
[28] S. Pasebani, M. Ghayoor, S. Badwe, H. Irrinki, and S. V. Atre, "Effects of atomizing media and post processing on mechanical properties of 17-4 PH stainless steel manufactured via selective laser melting," *Additive Manufacturing*, vol. 22, pp. 127-137, 2018, doi: 10.1016/j.addma.2018.05.011.
[29] D. Herzog, V. Seyda, E. Wycisk, and C. Emmelmann, "Additive manufacturing of metals," *Acta Materialia*, vol. 117, pp. 371-392, 2016, doi: 10.1016/j.actamat.2016.07.019.
[30] R. M. Kelkar, "High Quality Spherical Powders for Additive Manufacturing Processes Along With Methods of Their Formation," ed: Google Patents, 2019.
[31] R. Li, Y. Shi, Z. Wang, L. Wang, J. Liu, and W. Jiang, "Densification behavior of gas and water atomized 316L stainless steel powder during selective laser melting," *Applied Surface Science*, vol. 256, no. 13, pp. 4350-4356, 2010, doi: 10.1016/j.apsusc.2010.02.030.
[32] B. K. Nagesha, V. Dhinakaran, M. Varsha Shree, K. P. Manoj Kumar, D. Chalawadi, and T. Sathish, "Review on characterization and impacts of the lattice structure in additive manufacturing," *Materials Today: Proceedings*, vol. 21, pp. 916-919, 2020, doi: 10.1016/j.matpr.2019.08.158.
[33] V. V. Popov, A. Katz-Demyanetz, A. Garkun, and M. Bamberger, "The effect of powder recycling on the mechanical properties and microstructure of electron beam melted Ti-6Al-4 V specimens," *Additive Manufacturing*, vol. 22, pp. 834-843, 2018, doi: 10.1016/j.addma.2018.06.003.
[34] S. B. Park, B. Road, and U. Kingdom, "Investigating the effects of multiple re-use of Ti6Al4V powder in additive manufacturing," *Renishaw plc*, pp. 1-10, 2016.
[35] C. Rock *et al.*, "The Influence of Powder Reuse on the Properties of Nickel Super Alloy ATI 718™ in Laser Powder Bed Fusion Additive Manufacturing," *Metallurgical and Materials Transactions B*, vol. 52, no. 2, pp. 676-688, 2021, doi: 10.1007/s11663-020-02040-2.
[36] H. P. Tang, M. Qian, N. Liu, X. Z. Zhang, G. Y. Yang, and J. Wang, "Effect of Powder Reuse Times on Additive Manufacturing of Ti-6Al-4V by Selective Electron Beam Melting," *Jom*, vol. 67, no. 3, pp. 555-563, 2015, doi: 10.1007/s11837-015-1300-4.
[37] R. O'Leary, R. Setchi, P. Prickett, and G. Hankins, "An investigation into the recycling of Ti-6Al-4V powder used within SLM to improve sustainability," *InImpact: The Journal of Innovation Impact*, vol. 8, no. 2, p. 377, 2016.

[38] A. T. Sutton, C. S. Kriewall, S. Karnati, M. C. Leu, and J. W. Newkirk, "Characterization of AISI 304L stainless steel powder recycled in the laser powder-bed fusion process," *Additive Manufacturing,* vol. 32, p. 100981, 2020.

[39] S. E. Brika, M. Letenneur, C. A. Dion, and V. Brailovski, "Influence of particle morphology and size distribution on the powder flowability and laser powder bed fusion manufacturability of Ti-6Al-4V alloy," *Additive Manufacturing,* vol. 31, 2020, doi: 10.1016/j.addma.2019.100929.

[40] B. Liu, R. Wildman, C. Tuck, I. Ashcroft, and R. Hague, "Investigation the effect of particle size distribution on processing parameters optimisation in selective laser melting process," in *2011 International Solid Freeform Fabrication Symposium*, 2011: University of Texas at Austin.

[41] V. Contaldi, F. Del Re, B. Palumbo, A. Squillace, P. Corrado, and P. Di Petta, "Mechanical characterisation of stainless steel parts produced by direct metal laser sintering with virgin and reused powder," *The International Journal of Advanced Manufacturing Technology,* vol. 105, no. 7-8, pp. 3337-3351, 2019, doi: 10.1007/s00170-019-04416-4.

[42] L. C. Ardila *et al.*, "Effect of IN718 Recycled Powder Reuse on Properties of Parts Manufactured by Means of Selective Laser Melting," *Physics Procedia,* vol. 56, pp. 99-107, 2014, doi: 10.1016/j.phpro.2014.08.152.

[43] V. Seyda, N. Kaufmann, and C. Emmelmann, "Investigation of Aging Processes of Ti-6Al-4 V Powder Material in Laser Melting," *Physics Procedia,* vol. 39, pp. 425-431, 2012, doi: 10.1016/j.phpro.2012.10.057.

[44] G. Soundarapandiyan, C. Johnston, R. H. Khan, B. Chen, and M. E. Fitzpatrick, "A technical review of the challenges of powder recycling in the laser powder bed fusion additive manufacturing process," *The Journal of Engineering,* vol. 2021, no. 2, pp. 97-103, 2021.

[45] F. Ahmed *et al.*, "Study of powder recycling and its effect on printed parts during laser powder-bed fusion of 17-4 PH stainless steel," *Journal of Materials Processing Technology,* vol. 278, 2020, doi: 10.1016/j.jmatprotec.2019.116522.

[46] C. S. Kriewall, A. T. Sutton, S. Karnati, J. W. Newkirk, and M.-C. Leu, "Effects of area fraction and part spacing on degradation of 304L stainless steel powder in selective laser melting," 2017.

[47] R. W. Bochuan Liu, Christopher Tuck, Ian Ashcroft, Richard Hague "Investigation the effect of particle size distribution on processing parameters optimisation in selective laser," 2011, doi: http://dx.doi.org/10.26153/tsw/15290.

[48] G. Jacob, C. U. Brown, M. A. Donmez, S. S. Watson, and J. Slotwinski, 2017, doi: 10.6028/nist.Ams.100-6.

[49] H. Asgari, C. Baxter, K. Hosseinkhani, and M. Mohammadi, "On microstructure and mechanical properties of additively manufactured AlSi10Mg_200C using recycled powder," *Materials Science and Engineering: A,* vol. 707, pp. 148-158, 2017, doi: 10.1016/j.msea.2017.09.041.

[50] A. Gatto, E. Bassoli, and L. Denti, "Repercussions of powder contamination on the fatigue life of additive manufactured maraging steel," *Additive Manufacturing,* vol. 24, pp. 13-19, 2018, doi: 10.1016/j.addma.2018.09.004.
[51] M. Horn *et al.*, "Influence of metal powder cross-contaminations on part quality in Laser Powder Bed Fusion: Copper alloy particles in maraging steel feedstock," *Procedia CIRP,* vol. 94, pp. 167-172, 2020.
[52] G. Raugel and Y. Yi, "Professor Klaus Kirchgässner," *Journal of Dynamics and Differential Equations,* vol. 27, no. 3-4, pp. 333-334, 2015, doi: 10.1007/s10884-015-9497-z.
[53] I. Astm, "ASTM E8/E8M-16a: Standard Test Methods for Tension Testing of Metallic Materials," *West Conshohocken, PA, USA: ASTM International,* 2016.
[54] S. ASTM, "E466-15," *Standard Practice for Conducting Force Controlled Constant Amplitude Axial Fatigue Tests of Metallic Materials*.
[55] A. f. d. n. (afnor), "Essais de fatigue Traitement statistique des données," p. 48, Septembre 1991.
[56] I. M. W. Ekaputra, R. T. Dewa, G. D. Haryadi, and S. J. Kim, "Fatigue Strength Analysis of S34MnV Steel by Accelerated Staircase Test," *Open Engineering,* vol. 10, no. 1, pp. 394-400, 2020, doi: 10.1515/eng-2020-0048.
[57] P. M. Snyder, M.-W. Lu, and Y.-L. Lee, "Reliability-based fatigue strength testing by the staircase method," SAE Technical Paper, 0148-7191, 2004.